Magmatic systems

Aksyuk A. M., Konyshev A. A. Study of solidus parameters of the Yaroslavka biotite and Voznesenka Li-F granites of the Primorye, experimental research

Institute of Experimental Mineralogy of RAS, Chernogolovka
aksyuk@iem.ac.ru; konyshev@iem.ac.ru

Presents and discusses the experimental data obtained by the authors on the study of solidus of natural biotite and lithium-fluorine granites from the Voznesenka ore node in the Primorye. According to geological data these granites are close in age and belong to the Voznesenka complex. Biotite granites compose, apparently, the first phase, and Li-F – the second phase of the granites. This is confirmed by the experimental data, as solidus of biotite granite goes at higher temperatures at pressures below 300 MPa than solidus of lithium-fluorine granite, therefore, the last should have been for crystallize at lower temperatures. According to the mineral geofluorimeters the Li-F granites are characterized by high concentrations of fluoride in granite fluid, which is close to the typical Li-F granites of the Ta–Nb Orlovka and Etyka deposits in East Transbaikalia. The same deposits met and in the Voznesenka ore node. Solidus granite was studied experimentally in fluid with different fluoride concentrations. Fluorine contents were measured in the melt after experiments.

Key words: experiment, granite, solidus, fluorine, Yaroslavka, Voznesenka.

Reference: Aksyuk, A .M., A. A. Konyshev (2012), The study of solidus parameters of Yaroslavka biotite and Voznesenka Li-F granites of the Primorye, experimental research. *Vestnik ONZ RAS, 4, (doi:)*

On the territory of the Voznesenska ore node, located on the South-West Primorye known fluorite, Ta, Sn, W, Be and other deposits, the formation of which is associated with Voznesenka granite complex. To this complex include two phases: biotite and litium-fluorine granites. According to geological data these granites are close in age and belong to the Voznesenka complex, but the biotite granite composes, apparently, the first phase, and Li-F – the second one. This is confirmed by the experimental data, as solidus of biotite granite takes place at higher temperatures than one of lithium-fluorine, therefore, the last should have been for crystallize at lower temperatures.

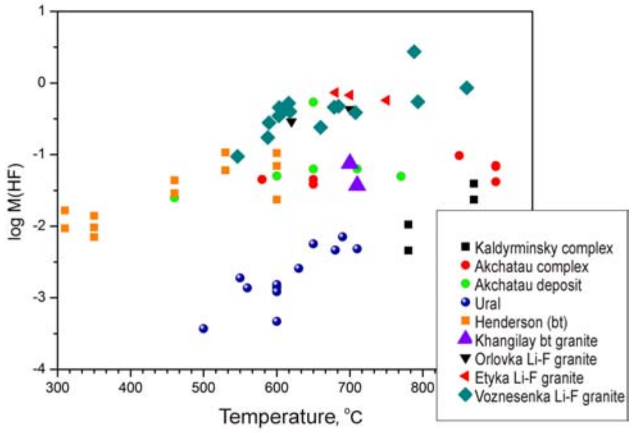

Fig. 1. Concentration of HF (M, mole/dm^3) in fluids of Voznesenka Li-F granites, defined with mineral geofluorimeters

According to the mineral geofluorimeters [*Aksyuk, 2002*] Li-F granites are characterized by high concentrations of fluoride in granite fluid of the Voznesenka ore node [*Ryazantseva, etc., 1994; Rub, Rub, 2006*]. Interestingly, these data are close to a typical concentrations of HF for Li-F granites of the Ta–Nb deposits Orlovka and Etykaa in East Transbaikalia (Fig. 1), which confirms the genetic affinity rare metal deposits of Voznesenka ore node and Eastern Transbaikalia. The increased concentration of fluorine in the melt and granite fluid leads to a shift of the melt composition to Li-F granite or greisens for already crystallized biotite granite, that explains the attribution by geologists them to one Voznesenka granite in view of the bad nakedness of the region.

According to experimental data solidus of biotite granites under pressure of 500 MPa are moving closer to the solidus of Li-F granite, which takes place at temperatures below or close to 600°C (Fig. 2).

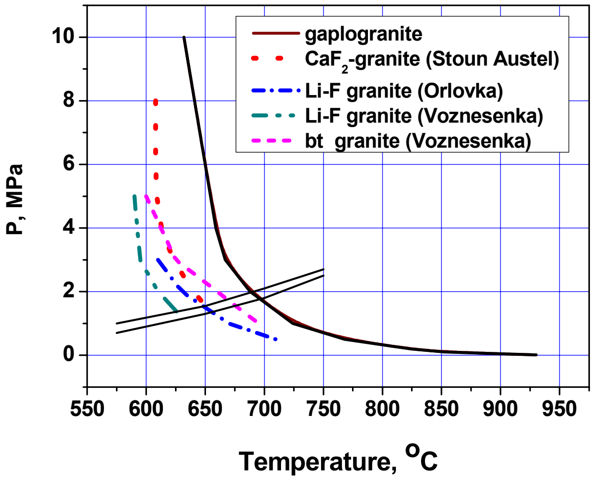

Fig. 2. Solidus of the Voznesenka biotite and Li-F granites in comparison with solidus of other granites

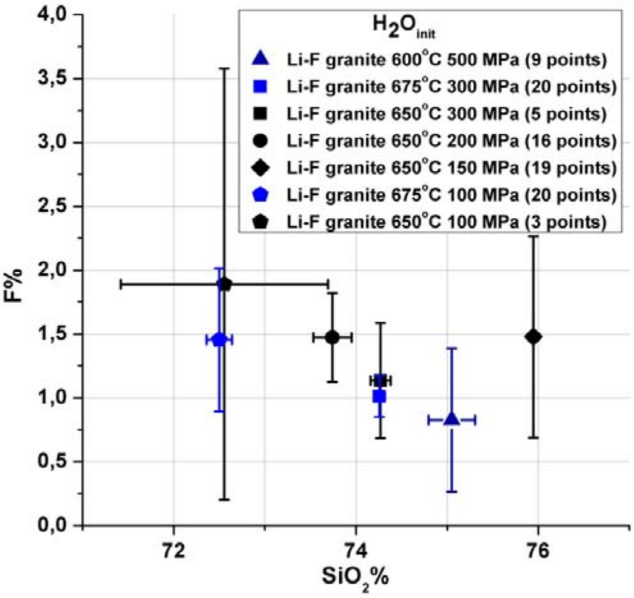

Fig. 3. The contents of F and SiO$_2$ (wt %) in glass of the Li-F granites after melting in H$_2$O

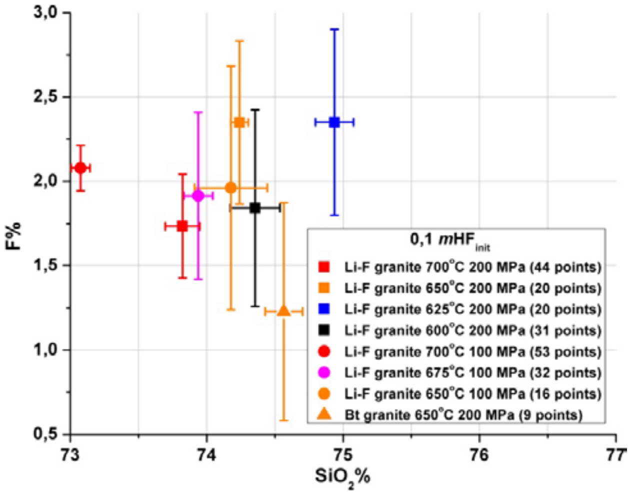

Fig. 4. The contents of F and SiO_2 (wt %) in glass of the Li-F and the Bt granites after melting in 0.1 m_{HF} initial

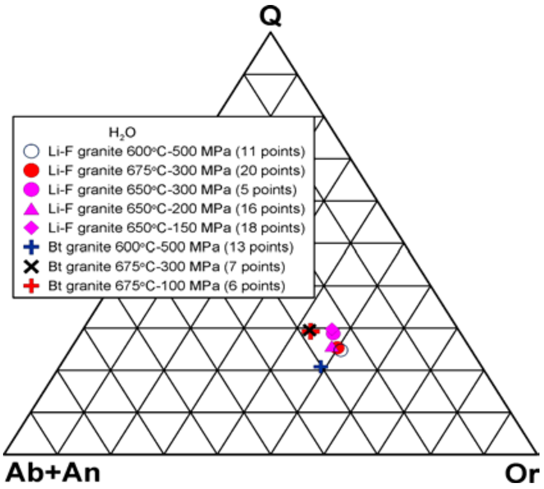

Fig. 5. Ab+Aq, Q, Or (wt %) in glass of the Li-F and Bt granites after melting in water

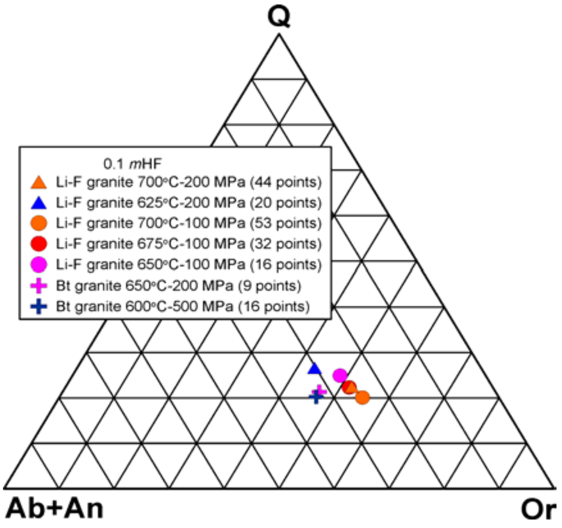

Fig. 6. Ab+Aq, Q, Or (wt %) in glass of the Li-F and Bt granites after melting in 0.1 m_{HF} initial

In the experiments with water content of F in the glass of Li-F granite is an average of 1–2 wt % according to the microprobe analysis (Fig. 3). In the ons with 0.1 m_{HF} it is on average 1–2.5 wt % F (Fig. 4). The contents of SiO_2 and F are were in the original granite on the data of x-ray-fluorescent analysis in the Li-F granite – 71.1 wt % SiO_2 and 1.3 wt % F, and in the Bt granite – 71.0 wt. % SiO_2 and 0.3 wt % F. Thus, after experiments content of F in the glass, and especially SiO_2 were noticeably increased.

Although the accuracy of the determination of fluoride on a microprobe in glasses was relatively high, but, all the same, the main measured values were slightly higher than the baseline granite, i.e. the melting granites several accumulate fluoride and silica in the glass. From the results of the conversion of the experimental glass on normative compositions can be seen that the compositions of glass shifts to the side of the Or corner, and, for Li-F granite a little more (Fig. 5 and 6).

The work was supported by RFBR grant 10-05-00292 and Program ONZ-3.

References:

1. Aksyuk, A. M. (2002). Experimentally calibrated geofluorimeters and estimation of fluoride in granite fluids, *Petrology*, v. 10, N 6, p. 628–642 (in Russian).
2. Ryazantseva, M. D., N. S. Gerasimov, I. N. Govorov (1994). Rubidium- strontium isochrone and petrogenesis of magmatic rocks of Voznesenka ore district (Primorye region), *Pacific Geology*, N 4, p. 60–73 (in Russian).
3. Rub, A. K., M. G. Rub (2006). Rare-metal granites of the Primorye, VIMS, M., 86 p. (in Russian).

Aksyuk A.M., Korzhinskaya V. S. Experimental study of greisenization of granite in water and HF solution at 400–600°C

Institute of Experimental Mineralogy RAS, Chernogolovka, Russia
aksyuk@iem.ac.ru; vkor@iem.ac.ru

An experimental simulation of greisenization of the voznesenka biotite and lithium-fluorine granites at 400–600ºC and 100 MPa in water and water-fluoride fluids showed that during the experiments, the sharp frontal diffusion of substitution did not occur in powder rocks, as observed in the dissolution of the individual grains and the formation of new minerals. There was "infiltration" process in a confined space capsule. According to microprobe analysis that is due to the relatively high porosity of the initial powders (tens of %) and the gradient of the component concentrations in the pore solution, as opposed to natural processes, where the porosity is usually up to 2–5 %. The results of analyzes of solid products, the experiments shown that the "metasomatic" alteration of granites in the course of the experiments clearly observed, depending on experimental conditions, but clearly apparent statistically.

Keywords: [experiment, greisenization, granite, fluorine, Voznesenka]

Reference: Aksyuk, A. M., V. S. Korzinskaya (2012). Experimental study of greisenization of granite in water and HF solution at 400–600ºC, *Vestnik ONZ RAS, 4,* (doi:)

Greisenization rare-metal granite is a widespread process in nature and develops in the form of rims for cracks in the granite, quartz-filled, with a hydrothermal process. In the fluid-magmatic stage in the rare-metal granites, especially with the fluorine-rich fluid, evolving "avtometasomatoz" primarily in the apical parts of the ledges of granite massifs, which are sometimes formed thick zones greisenizaed granites. On the territory of the Voznesenka ore area (in the Primorye) are known different (Ta–Nb, W, Sn, etc.) deposits which formation are associated with granites greisenization of the voznesenka complex. The complex includes two phases: biotite and lithium-fluorine granites. Li-F granite make up a small (1–2 km) stocks, which are igneous or independent body, or transformed and greisenized projections underlying the more powerful (more than 10 km in diameter) of the massif of biotite granite. The source of ore-bearing fluids was a deep magma chamber. Fluoride has played a major role in the formation of greisen and greisen deposits of the Voznesenka area. According to our estimates obtained using geofluorimeters [*Aksyuk, 2002*], in fluid of the granite the concentration of fluoride was about 0.1–1 mHF. From the physicochemical point of view greisenization granites is, first and foremost, the reaction of hydrolysis of feldspars and their replacement by quartz-mica-topaz. Transformations of biotite granites under the influence of fluoride fluids at high P-T conditions bring them closer to the composition of lithium- fluorine granites.

Greisen zoning in granites simulated experimentally by *G.P. Zaraisky* [*1989*]. We have performed experiments on the formation of greisen in endocontact of voznesenka biotite and Li-F granites, which were carried out in autoclaves with automatic temperature control during the experiment. In an autoclave were placed containers sealed, lined with platinum, inside which an open platinum or quartz ampoule. Internal volume of the container was about 20 cm^3. Open platinum or quartz ampoule was jammed mashed powder of granite weighing about 0.3-0.4 g and container was filled with an aqueous solution of a given concentration of HF. Rock-fluid ratio was about 1:25. The duration of the experiments was 15–30 days.

After the experiment products of runs were impregnated and sealed with cyanoacrylate without destroying (Fig. 1), ground to the required depth and studied by x-ray (microprobe) Cam Scan MV2300 (VE GA TSS130MM).

Fig. 1. The columns after the experiment

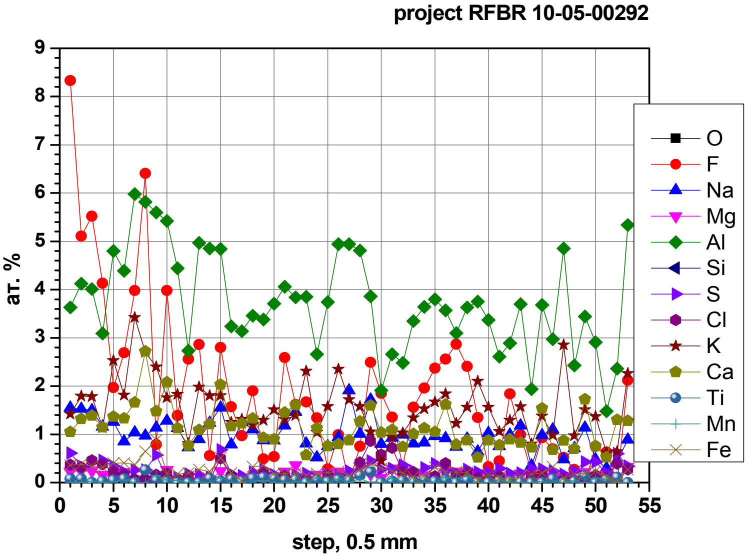

Fig. 2. The composition of the column at 600°C, H_2O

Recording of spectra was carried out on areas with a side of about 0.5x0.5 mm in increments (steps) of approximately 0.1–0.5 mm. According to the microprobe analysis of the experimental greisen columns, a sharp frontal diffusion replacement of powder rocks was not observed, and there was the dissolution of the individual grains and the formation of new minerals. There was "infiltration" process in a confined space capsule. That is due to the relatively high porosity of the initial powders (tens of %) and the gradient of the component concentrations in the pore solution along the length of the column, as opposed to natural processes, where the porosity of the rock is usually up to 2–5 %.

Analysis of the composition of solid products of the experiments shows that the "metasomatic" alteration of granites in the course of the experiments clearly observed, depending on experimental conditions, but these relationships manifested statistically. This required measurements of rock compositions by the microprobe on sites with size we used the most often 0.5x0.5 mm.

At 600°C and 100 MPa in H_2O (Fig. 2, open to a solution on the left) and 1m HF solutions after the experiments the pH was shifted markedly to 2.2 in the water and 2.45 in 1m HF. In experiments of long duration (more than 30 days) crystals of potassium feldspar and albite are completely dissolved. In the platinum-lined canisters at 500°C and a pressure of 100 MPa, in 1m HF solutions contents of Al and F drastically changed in the column to open to solution end (Fig. 3, right).

The upper (open to solution) part of metasomatic columns were encountered clusters of grains of fluorite, some grains of sellaite (Mg (OH, F)$_2$), topaz, mica flakes with distinct cleavage, and quartz grains increased in size.

In experiments at 400–500°C and 100 MPa, 0.5 m_{HF} +0.5 m_{HCl} (Fig. 4, 5), albite and K-feldspar also completely dissolved and the chemical composition of granite dramatically changed.

Sometimes the inside of the column began to form quartz veins. At the open end of the metasomatic column formed separate grains hieratite (K_2AlSiF_6), elpasolite (K_2NaAlF_6). Voznesenka Li–F granites throughout the column converted to zwitter (quartz + topaz). There were retained only rare grains of oxides Fe, Ti and Ta–Nb and sometimes preserved grains of zircon with Zr/Hf ratio of 13-17 typical to high evolved granite. Biotite granite in front of the column converted to zwitter over one third of length, where among the remaining and newly formed grains of quartz crystals grows F-topaz. Then instead of the topaz were formed andalusite, which is marked on the Voznesenka fields. The initial solution (0.5 m_{HF} +0.5 m_{HCl}) had pH = 1.45.

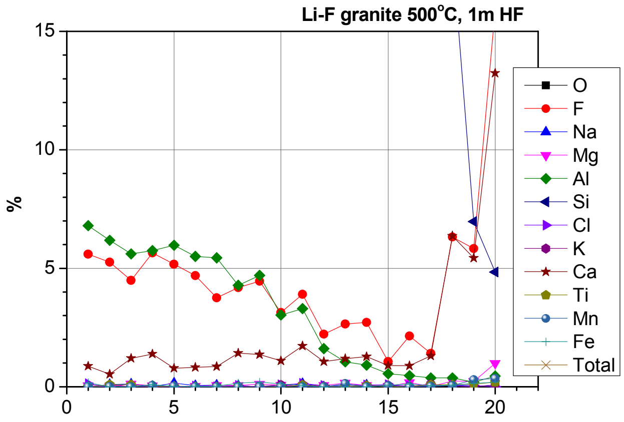

Fig. 3. Greisen column by voznesenka Li-F granites (open to the solution of the-right)

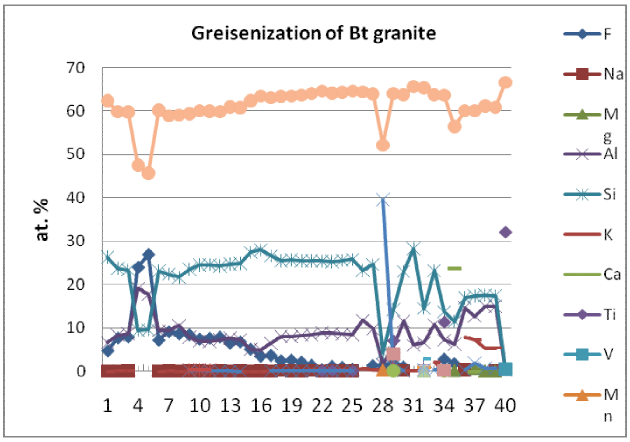

Fig. 4. Greisenization of biotite granite, measured in 1 mm increments (open to the solution of the columns is at the left)

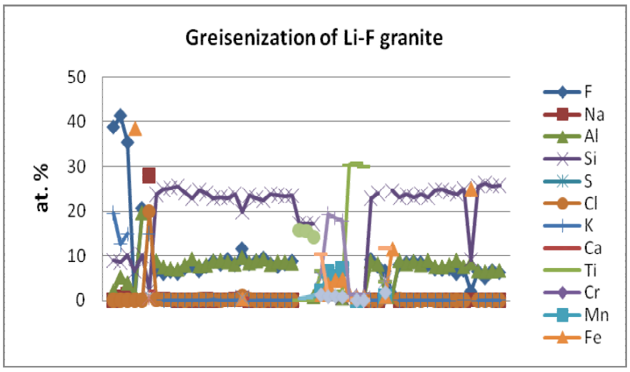

Fig. 5. Greisenization of Li-F granite, measured in 1 mm increments (open to the solution of the columns is at the left)

After the runs with the Li–F granite, it has changed to pH 1.69, with the biotite granite it was up to pH = 1.80. This indicator has changed little during the experiment. The concentration of fluoride in quenched solution was m_F = 0.0155 mol/kg H_2O for the Li-F granites and m_F = 0.0204 mol/kg H_2O for the biotite granite. Fluoride solutions in granitic fluids voznesenka ore district contributed to the dissolution and transport of tantalum-niobates in the endocontact aureole. According to mineralogical data [*Lugovskoy, 1968*] on the Voznesenka ore field there was developed tantalbearing struverite $(Ti,Ta,Fe)_3O_6$), which is present in the predominantly ferric iron. This indicates the important role of redox conditions during formation its, that is confirmed by our experimental data on the solubility of tantalum-niobium minerals [*Korzhiskaya, Kotova, 2012*].

This work was supported by RFBR Grant № 10-05-00292/

References:

1. Aksyuk, A. M. (2002). Experimentally calibrated geofluorimeter and estimation of fluorine concentration in granitic fluids, *Petrology*,. v. 10, No 6, pp. 628–642 (in Russian).
2. Korzhinskaya, V. S., N. P. Kotova (2012). The role of hydrothermal-metasomatic factors in the formation of deposits tantaloniobate deposits, *Scientific Conference. Theoretical issues and research practices of metasomatic rocks and ores. Abstracts*, Kiev, p. 41–42 (in Russian).
3. Lugovskoy, G. P. (1968). Geology, mineralogy, geochemistry, and conditions for the formation of granites tantalbearing. M. Funds of VIMS. 247 p. (in Russian).
4. Zaraisky, G. P. (1989). Zoning and conditions for the formation of metasomatic rocks. Moscow, Nedra, 348 p. (in Russian).

Asavin A.M., Turin D.A., Senin V.G. Experimental measurement coefficient distribution TR, Ni, Mn melilite-melt

V. I. Vernadsky Institute of Geochemistry and Analytical Chemistry RAS, Moscow *aalex06@inbox.ru*

The paper discusses the distribution coefficients of trace elements obtained in the experimental melting of melilitic melts containing between pyroxene-melt and melilite-melt. The data on the distribution of Zr, Hf, TR, Ni, Co, Mn compared with the estimates of the distribution coefficients in natural melilite-bearing porphyritic volcanic rocks. Comparison of the data and analysis of literary sources suggest the possibility of changing ratios Zr/Hf, Th/U, Ni/Co in the fractionation of melilite and pyroxene in the high-Ca alkaline melts.

Key word: [distribution coefficients of trace elements, melilite, alkaline magma differentiation]

Reference: Asavin, A. M., D. A. Turin, V. G. Senin (2012), Experimental measurement coefficient distribution TR, Ni, Mn melilite-melt, *Vestnik ONZ RAN, 4*

One of fundamental problems of geochemistry is genesis and formation conditions larnite-normative magmas. Interest to this type of magmas is caused by that of large-scale deposits is closely connected with them (Kovdor, the Gulinsky intrusion, Afrikanda). In paragenesis with them carbonatite complexes are observed, also. Subvolcanic rocks of such type quite rare. The most known regions where they are widespread it the African province central rift [Gerasimovsky & Polikov, 1974; Bailey et al., 2005] and Maymecha Kotuiy province [Juk Pochekutov et. al., 1975; Butakova & Egorov, 1962; Egorov, 1969; Rass, 2008], the Kola (Turiy Peninsula) province [Ivanikov et al 1998, Beard et al., 1998, Dunworth & Bell 2003, Arzamastsev, et al 2009], the Rhine graben [Hegner et al., 1995; Wilson et al., 1995; Dunworth & Wilson, 1998, Ulianov et al., 2007]. The same type found from the oceanic islands. They are presented on Trindade islands, Cape Verde, Fernando de Noronha, Hawaii, Gran Canary. The assessment of coefficient distribution (Kd) of trace elements for these liquids represents considerable interest as for understanding of processes of a fractionation of trace elements, and for an assessment of influence of a high alkaline melts on the variation Kd value.

We investigated several natural samples porhyritic melilitites (Ol, Mell, ±Cpx as porphyric-crystal) (African and Maimecha Kotuyi province), and spent several isothermal experiments, with the melt close to turyaite and melilitite (sample 11073).

Table 1. Composition of the rock (val) and groundmass (om) and glass (Liq) in micro inclusion in porphyric mineral

Sample	phase	SiO_2	TiO_2	Al_2O_3	FeO	MnO	MgO	CaO	Na_2O	K_2O	P_2O_5	Sum
87_50	val	36.52	1.77	12.07	10.14	0.143	8.65	20.57	5.24	2.09	0.44	98.96
87_51	val	34.97	2.47	8.78	10.31	0.234	25.86	11.17	3.83	0.349	0.416	99.08
87_51	om	36.24	2.46	9.75	10.77	0.27	24.68	10.68	2.485	0.92	0.045	98.58
87_51	om	35.85	2.92	9.06	10.43	0.265	26.78	11.78	1.25	0.87	0.028	99.51
87_49	val	39	1.94	11.94	8.696	0.11	9.19	16.61	5.58	1.526	0.178	98.43
87_49	om	38.07	2.18	11.49	9.42	0.114	9.4	21.16	4.52	1.37	0.084	99.26
87_49	Liq	36.2	3.5	2.62	23.41	0.085	0.64	33.5	0.011	0.018		99.83
87_49	Liq	33.5	8.76	2.71	20.18	0.069	1.39	33.3	0.0237	0.007		101.42
87_48	val	37.25	2.24	10.88	10.29	0.13	8.65	20.37	4.18	1.55	0.13	101.42
87_48	om	44.11	0.015	8.716	2.564	0.1	7.66	33.32	3.426	0.081		98.98
87_48	om	43.93	0.018	8.283	2.46	0.099	8.13	33.89	3.04	0.089		100.39
87_48	Liq	40.62	5.237	16.05	6.31	0.009	16.74	9.72	1.928	2.87		100.21
87_48	Liq	40.73	5.202	15.58	6.69	0.04	15.44	12.32	1.914	1.66		101.49
87_48	Liq	40.89	5.015	15.33	6.51	0.044	15.93	12.48	1.94	1.56		99.43
87_48	Liq	51.96	0.415	7.75	4.86	0.11	17.23	16.3	0.986	0.077		100
0014	om	41.18	3.16	6.94	12.7	0.167	12.15	10.94	3.4	2.17	0.56	98.07
0014	val	39.08	1.896	6.82	12.49	0.146	15.6	15.2	3.48	2.05	0.67	99.93
0014	val	38.88	1.857	6.69	12.46	0.156	15.75	15.12	3.47	2.02	0.656	99.56
turiyte	val	41.84	3.18	7.4	13.03	0.21	14.64	15.34	2.25	2.07		99.96
11073	val	41.14	9.697	3.25	10.93	0.132	9.88	11.44	1.93	4.901	0.96	97.93
11073	om	39.22	8.54	1.79	13.58	0.18	16.11	14.54	2.24	1.82		98.02
11512	val	34.86	7.05	4.034	12.3	0.191	15.07	16.12	1.44	4.07	1.028	98.78
11512	om	40.53	9.21	3.41	11.32	0.141	9.89	11.81	2.24	5.345	1.147	97.83
11511	val	35.8	6.87	4.079	12.13	0.187	14.32	16.5	1.5	3.5	1.014	99.31
11515	val	36.31	7.25	3.827	11.84	0.183	15.53	15.59	1.27	3.76	0.986	100.07
M6538	val	40.58	9.72	2.59	0.057	11.6	0.126	10.39	14.61	3.74	1.186	98.66

Table 2. Composition (wt. %) porphyric-minerals from melilitic volcanic rock.(Melilite calculate on the 5 cations and 7 oxygen xAk – akermanite, xGe – gelenite, xNaGe – Na-melilite, xFeAk –ferric-akermanite)

Mineral	Clinopyroxene (Cpx)	Melilite (Mell)							
Sample	11073	87_48							
SiO_2	51.5.	39.04	38.49	37.87	38.96	44.97	45.06	44.23	44.59
TiO2	1.5	0.06	0.09	0.04	0.10	0.00	0.03	0.01	0.00
Al_2O_3	3.5	14.85	11.71	16.98	16.59	8.34	8.35	8.59	8.08
FeO	4.51	5.70	13.71	3.91	4.37	1.66	2.60	2.69	2.37
MnO	0.1	0.01	0.12	0.07	0.07	0.06	0.04	0.05	0.04
MgO	15.5	3.74	0.21	3.84	3.47	8.27	7.61	7.70	7.98
CaO	23.5	36.48	35.56	37.00	36.38	33.25	32.91	33.31	33.61
Na_2O	0.5	0.04	0.04	0.08	0.06	3.39	3.33	3.34	3.27
K_2O		0.03	0.03	0.18	0.00	0.04	0.08	0.09	0.07
NiO		0.026	0.028	0.041	0	0.03	0	0	0
Total	100.6	100.57	101.35	100.33	100.41	100.09	100.25	100.24	100.22
xAk						59.9	55.5	54.9	58.5
xGe						8.5	8.9	9.6	8.3
xNaGe						34.3	34.1	33.8	32.9
xFeAk						7.3	11.5	11.8	10.3
Sum cation						5.2	5.2	5.2	5.2

The complexity of the fractionation melilitic magma due to the presence of a phase system describing the crystallization of high-calcium silica undersaturated magmas peretektic reactions [Schairer et al., 1962, Yoder, 1967, Gee & Sack 1988]:

$$\mathrm{Mell(Ca_2MgSi_2O_7) + Ol(Mg_2SiO_4) + Liq(NaAlSi_3O_8) \leftrightarrow Cpx(CaMgSi_2O_6) + Ne(NaAlSiO_4)} \quad (1)$$

$Ne(KAlSiO4) + Liq(SiO2) \leftrightarrow Lc(KAlSi_2O_6)$ (2)

$Mell(Ca_2MgSi_2O_7) + Ol(Mg_2SiO_4) \leftrightarrow Cpx(CaMgSi_2O_6) + Mo(CaMgSiO_4)$ (3)

Table 3. Product of the run with and condition

№ run	Time duration (hour)	T°C	Phase composition	% vol. of Glass in product of run
	Melilite nephelinites -11073			
06	88	1260	Liq–Ol–Mgt	
05	92	1230	Liq–Ol–Mgt	
02	48	1212	Liq–Ol–Cpx–Mgt+Bd	
04	94	1180	Liq–Ol–Cpx–Mgt+Bd	
08	111	1165	Liq–Ol–Cpx–Mgt+Bd	
03	157	1150	Liq–Ol–Cpx–Mgt+Bd	
			Turiyte	
7,8	24	1250	Liq–Ol–Mgt	90

Besides the main phase of the crystallizing – melilite (Mell), pyroxene(Cpx), have a variable composition, broad miscibility of components, which increases the uncertainty of estimates of the residual melts during fractionation. The compositions of the investigated natural volcanic rocks in the diagram Ln–Fo–An are located close to the lines of these peretectic reactions line and cotectic Ol–Mell and Cpx–Ol (Fig.1). At C point the melt is saturated with melilite and olivine begins to react with the formation of pyroxene and olivine in the process of reaction removes in the direction to point D (content of Ol decrease). In the field of point C is the thermal barrier (Ab–Di peretectic) separates the melilite-pyroxene melts from nepheline-pyroxene. The position of this point is not very defined (the approximate temperature in model systems 1140C°). It is essential important that, depending on the conditions and of the primary melt composition the differentiation trend can go in different directions toward a more high-Ca and potassic melts with melilite and vollastonite (point D), or to less alkali feldspar phonolitic volcanic rock to the end. It is interesting to note that the investigated samples are African right of the point and therefore fractionated by phonolitic trend, whereas samples Maimecha Kotuiy province provide a more alkaline and undersaturated trend.

We conducted experiments with molten melilite-nephelinites (sample 11073) and turyiate. For isothermal experiments used a tube furnace design L. D. Krigman. Powders of the samples put in a platinum capsule with a diameter of 0.05 mm. The full weight of the mixture in the capsule was approximately 200 mg. Duration of exposure at a given temperature the equilibrium of experience ranged from 24 to 57 hours depending on temperature. Since the experiments were conducted at uncontrolled oxygen fugacity - the air, we evaluate it on up to buffer NNO+1 (buffer $Ni+O_2 = NiO$). In rock substance added Zr and Hf and other trace element in the form of aqueous solutions of a given concentration. The concentrations of trace elements have changed from 0.002 to 5 wt.%.

These mixtures were melted at temperatures above the liquidus to the complete melting of the charge (incubated for one hour) and then decrease to the temperature of the isothermal sections and incubated for an equilibrium mineral-melt. Exposure time was sufficient to achieve an equilibrium concentration between minerals and liquid. Our measurement of concentration profiles of Zr, Hf, Ca, Si, Al, Mg, Fe in the glasses showed a homogeneous distribution of crystals around the phenocrysts. In the experience of the products were available for analysis of melilite (Mell), olivine (Ol) clinopyroxene (Cpx), magnetite (Mgt) and glass (Liq). Result of the runs show in tabl.2.

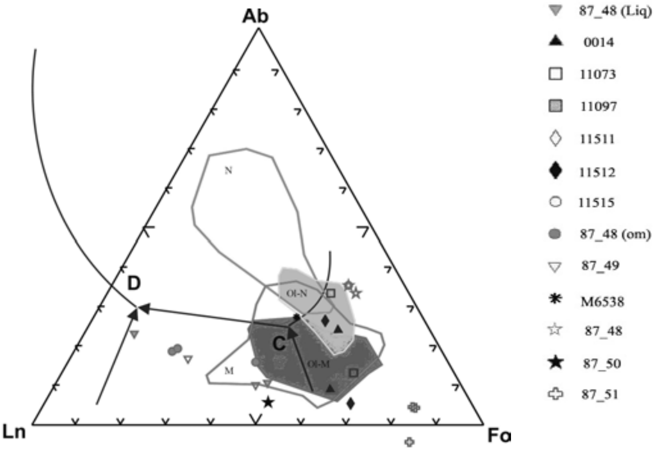

Fig. 1. Our data of melilitites in the diagram La–Ab–Fo [*Peterson, 1989*] Grey lines mark the fields: M – melilitites, Ol-N – olivine nephelinites (melanephelinite), Ol-M – melilitites olivine; N – nephelinites. Our formulations see the legend. Dark blue lines are pseudo-cotectic line and peretektic reaction: D-C (view in text).

The results of experiments were analyzed by microprobe, including those used in our specially designed technique for the analysis of low contents of Zr and Hf [Senin et al., 1989].

Analysis of the contents of TR in melilite from experiments with turiyte was carried out with a laser and spark mass spectrometry (SMS) [Ramendik et al., 1989].

Experiments have shown that in dry oxidizing conditions in the melilitic-nephelenite melts melilite does not crystallize. Only in the more undersaturated melts such as turiyte melilite crystallize. As the temperature falls the melt gets in the area of peretektic reaction - melilite is disappears, remains pyroxene. How will the change of Kd value in these conditions?

Clinopyroxene–melt equilibria

We found very high values Kd for Zr and Hf for the pyroxene-melt equilibria in the experiments with the nephelinites (fig.2).

Experimentally, Kd pyroxene- melilitite-rich melts virtually not been investigated. From the experimental data, we can mention the work [*Gaetani & Grove, 1995; Hill et al., 2000*] that show Kd increases with increasing TR content in the pyroxene end-member Chermak in high calcium melts. The values Kd of Zr and Hf obtained in [*Hill et al., 2000*] is also very high, and remains a big difference in the values of (almost an order of magnitude) between them. Also published several papers on the study of equilibria in the silica-undersaturated melts. For example, in [*Green et al., 1992; Sweeney et al., 1995; Klemme et al., 1995; Blundy & Dalton, 2000; Adam & Green, 2001*] surveyed the distribution of trace elements in pyroxene carbonatite melts, which can also be viewed as an analogue of high-calcium alkaline magmas. In [*Hill et al., 2000*] studied a model kimberlitic melt. With the exception of [*Klemme et al., 1995*] in these equilibria also seen a big difference between Kd of Zr and Hf values and also Kd value is higher than in the melts of normal alkalinity.

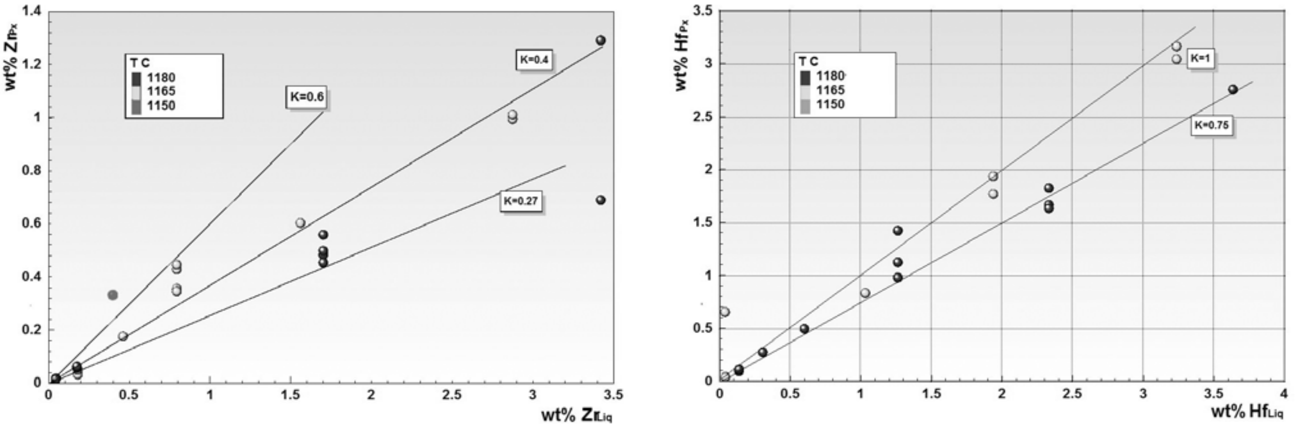

Fig. 2. Coefficient distribution pyroxene-melt of Zr and Hf in the different equilibrium temperatures

It is also very limited data on the Kd pyroxene of the in natural melilitic melts. We identified Kp for pyroxene in natural melilite-nepheline for sample 11073. At Fig.3 presents data on Kd in similar high-calcium melts with melilite, and our data. It is seen that the data on Kd vary widely.

In addition, there are a number of data for Kd in the natural lamproitic melts [*Foley, 1996; Foley & Jenner, 2004*]. Although the thatr melts usually have a specific composition - relatively high content of SiO2 and alkalis at low CaO.

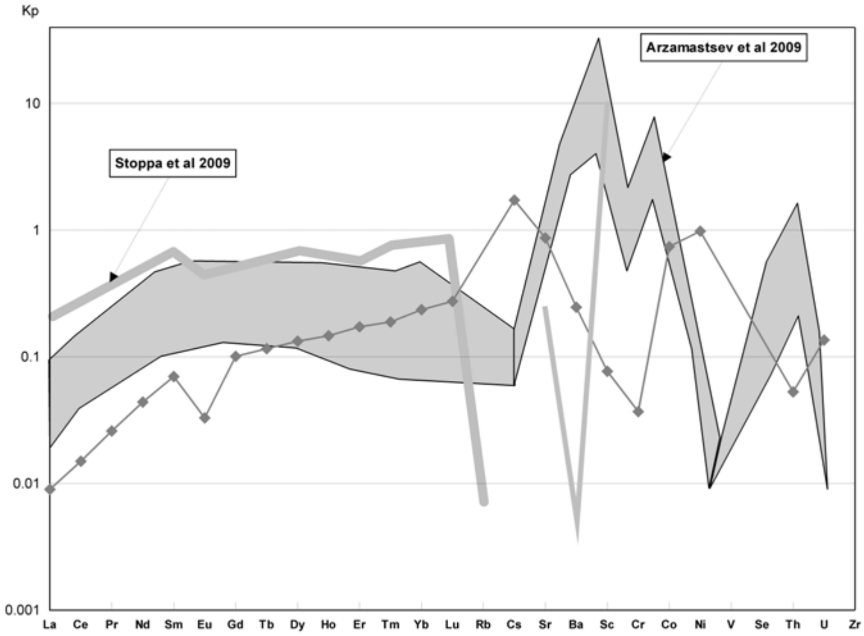

Fig.3. Kd pyroxene measured by us for sample 11073 (line with diamonds) and literature data: [*Stoppa et al., 2009*] for a range of Kd values for melilitic nephelinites – the wide gray line; [*Arzamastsev et al., 2009*] of the Turiy cape and melilite from the Kaiserstuhl - gray area

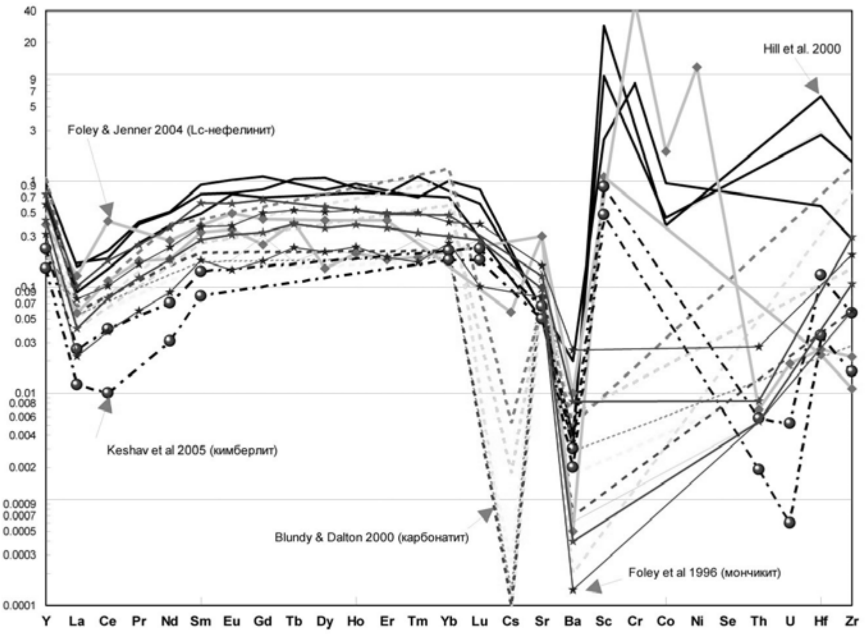

Fig. 4. Kd pyroxene from the literature: thin dashed lines – carbonatites [*Blundy & Dalton, 2000*], the black solid line – with a high content in pyroxene end-Chermak minal [*Hill et al., 2000*], black dash dotted line with a ball marker – an experiment with an analog kimberlite melt at a pressure of 6 GPa [*Keshav et al., 2005*]; line with asterisk markers, natural leucite nephelinite [*Foley & Jenner, 2004*]

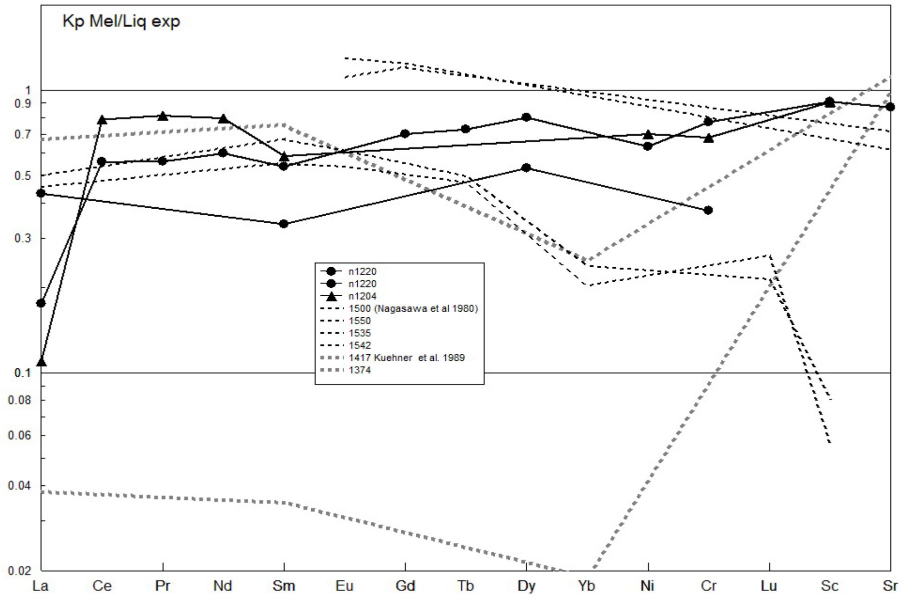

Fig. 5. Kd melilite in experiments on melting turiyte (black lines) measured by the SMS analysis. Addition experimental data [*Nagasawa et al., 1980, Kuehner et al., 1989*].

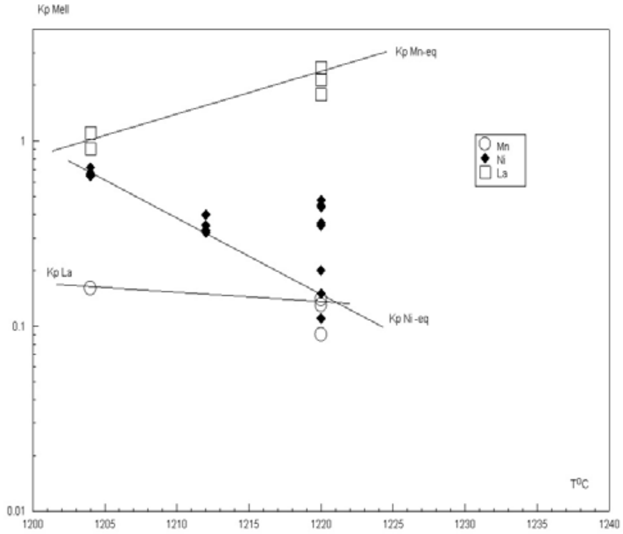

Fig. 6. Kd melilite in experiments with turiyte (lines indicate trends of change of Kd) measured by the microprobe analysis

The data on the natural volcanic rocks are quite different from those obtained in experimental conditions. First the estimated Kd TR have the lowest values available in literature experimental Kd, second Kd heavy rare earths relatively light monotonically increases (the slope of the curve on the graph Kd is constant), in contrast to published data where from La to Sm Kd value increases the slope and then disappears, and for the Er–Lu may decrease the value of Kd.

In the third for our sample is characterized by a very minimum for Kd europium. Most similar to the results obtained for Kd kimberlite obtained at high pressure (6 GPa) [*Keshav et al., 2005*]. However, these experiments were conducted at high temperatures (decrease values of Kd), and in our case, we would expect higher value of Kd TR. Very big difference in the values Kd of Cr, Co, Ni. Our values are less than 1, and the literature contains a similar and much higher than 1 value.

Lithophile elements are also characterized by a very wide interval of Kd values. And often reveals a large difference between the paired trace elements. Basically Kd Hf > Zr >> Nb, Th > U. All this creates a great opportunity to change the relationship pair of trace elements during the fractionation process. Interestingly, in experiments [*Gaetani & Grove, 1995, Hill et al., 2000*] with pyroxenes that contain a high proportion of Chermak-component, obtained very high values Kd Zr and Hf greater than 1. Under such circumstances, perhaps even melt depletion of lithophile trace elements the last portion of the melt.

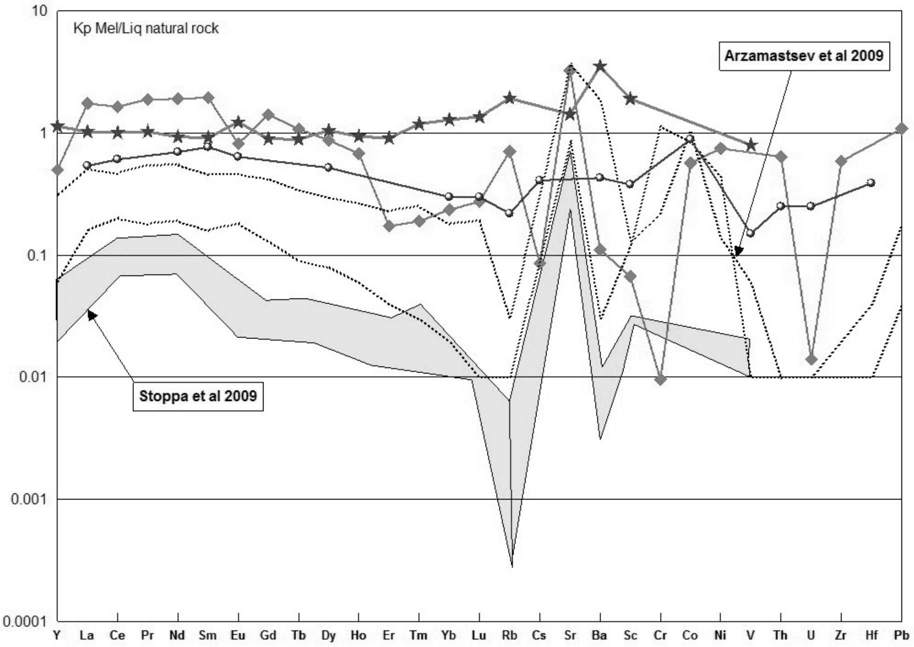

Fig. 7. Kd melilite measured us for sample 87_48 (black line with diamonds) and literature data: [*Stoppa et al., 2009*] gray box – a range of values for Kd melilitic nephelinites; and the line with the Stars – Kd melilite for melilitite–carbonatite lappilly; [*Arzamastsev et al., 2009*] point black lines – for turyaita Turego of the Cape and from the Kaiserstuhl melilitites;[*Onuma et al., 1981*] line with circular dots - Kd in Uganda from Zaire

Melilite–melt equilibria

Of great interest are the data we obtained for Kd melilite as the information on the quantities of this mineral Kd in natural melts is extremely small. Fig. 5 shows the measured by us in the turiyte Kd and a number of experimental data in the literature.

Our data are consistent with the highest values of Kd. They are close to the Kd rare earth elements from ugandite [*Onuma et al., 1981*] and they are approaching the magnitude of the Kd melilitite lappily tuff [*Stoppa et al., 2009*]. It is also interesting negative Eu anomalies and positive Rb. The high level of Kd values of the sample studied is shown in the considerably greater than 1 Kd Sr and high Kd Pb.

Our results are similar to the Kd from turiyte studied by [*Arzamastsev et al., 2009*]. It is interesting to note the relatively high (but low 1) the value Kd of Co, Ni, Zr. Significant difference between the Kd Th and U. An indirect confirmation of the availability of high Kd melilite for Fe-group elements and some lithophile elements are the data [*Petibon, 1999*]. In this paper for the equilibrium melilite - carbonatite melt obtained high Kd Th 0.52, Hf 0.11 Y 0.37.

Conclusion

Our investigation of Kd pyroxene and melilite in the high-calcium melts and analysis of data in the literature, above all, shows the poor knowledge of the distribution of trace elements in the crystal-melt equilibria in these magmas.

For quite certain established patterns can be attributed – a slight difference between the LTR and HTR Kd for clinopyroxene and an inverse relationship to melilite.

High Kd melilite TR and probably high Kd clinopyroxene (due to the increase in the concentration Chermak- minal) in general reduce the rate of accumulation of incompatible elements in the evolution of these magmas.

A very important feature is the significant difference in Kd lithophile elements. For melilite and pyroxene set a big difference between Th and U, Zr and Hf.

The peculiarity of the evolution of these melts is the presence of complex peretektic reactions (especially with the addition volatile component) between the crystallizing phases, kinetic factors are likely to lead to the prevalence of non-equilibrium in natural magmas associations. In this relatively low temperature equilibrium and a small difference between the temperatures and eutectic points peretektic reaction process make insignificant variations for Kd by the temperature factor. The greatest importance is the effect of melt composition, and changes in the composition of crystallizing phases (melilite, pyroxene).

It should be emphasized that the evolution of melilitic and nephelinite melts leads to the formation of alkaline agpaitic melts, which a strong change in the Kd values.

References:

1. Adam, J., T. Green (2001). Experimentally determined partition coefficients for minor and trace elements in peridotite minerals and carbonatitic melt, and their relevance to natural carbonatites*, European Journal of Mineralogy*, v.13 (5), pp.815–827.
2. Arzamastsev, A. A., L. V. Arzamastseva, Bea, F., Montero (2009). Trace elements in minerals as indicators of the evolution of alkaline ultrabasic dike series: LA–ICP–MS data for the magmatic provinces of northeastern Fennoscandia and Germany, *Petrologiya,* v.17, N.1, pp.51–78.
3. Bailey, K., F. Lloyd, S. Kearns, F. Stoppa, N. Eby, A.Woolley (2005). Melilitite at Fort Portal, Uganda: Another dimension to the carbonate volcanism, *Lithos*, v.85 (1–4 SPEC. ISS.), pp. 15–25.
4. Beard, A. D., H. Downes, E. Hegner, S. M. Sablukov and V. R. Vetrin, et al. (1998). Mineralogy and geochemistry of Devonian ultramafic minor intrusions of the southern Kola Peninsula, Russia: implications for the petrogenesis of kimberlites and melilitites, *Contributions to Mineralogy and Petrology*. v.130, N.3–4, pp.288–303
5. Blundy, J. and J. Dalton (2000). Experimental comparison of trace element partitioning between clinopyroxene and melt in carbonate and silicate systems, and implications for mantle metasomatism. *Contributions to Mineralogy and Petrology,* v.139: pp.356–371.
6. Butakova & Egorov (1962). Maimecha–Kotyi complex alkaline province alkaline and ultarabasic rocks. Cyrillic. *IN book: Petrography East Siberia. Siberia plate and their North border. M. Academy of USSA*., v. 1. pp. 417–587.
7. Dunworth, E. A. and K. Bell (2003). The Turiy Massif, Kola Peninsula, Russia: mineral chemistry of an ultramafic–alkaline–carbonatite intrusion, *Mineralogical Magazine*, v. 67(3), pp. 423–451.
8. Dunworth, E. A., M. Wilson, (1998). Olivine melilitites of the SW German Tertiary volcanic province: Mineralogy and petrogenesis, *Journal of Petrology*, v.39 (10), pp. 1805–1836.
9. Egorov, L.C. (1969). Melilitic rock of the Maimecha Kotyi province Cyrillic. *Trudy NIIGA*., т.169, 247c
10. Foley, S. and G. Jenner, (2004). Trace element partitioning in lamproitic magmas – the Gaussberg olivine leucitite. *Lithos*, v.75: 19–38.
11. Foley, S. F., S. E. Jackson, B. J. Fryer, J. D. Greenough, and G. A. Jenner (1996). Trace element partition coefficients for clinopyroxene and phlogopite in an alkaline lamprophyre from Newfoundland by LAM–ICP–MS *Geochimica et Cosmochimica Acta*, v.60 (4), pp. 629–638.
12. Gaetani, G. A. and T. L. Grove, (1995). Partitioning of rare earth elements between clinopyroxene and silicate melt Crystal–chemical controls, *Geochimica et Cosmochimica Acta*, v.59 (10), pp. 1951–1962.
13. Gee, L. L. and R. O. Sack (1988). Experimental Petrology of Melilite Nephelinites, *Jornal of Petrology*, v. 29, Pin 6, pp 1233–1255.
14. Gerasimovsky, V. I. & A. I. Polikov (1974). Geochemistry of volcanic rocks of the rift zones East Africa Cyrillic. *In the book East–Africa rift system M., NAYKA*, v.3 pp.5–194
15. Green, T. H., J.Adam, S.H. Siel (1992). Trace element partitioning between silicate minerals and carbonatite at 25 kbar and application to mantle metasomatism, *Mineralogy and Petrology*, v.46 (3), pp. 179–184.
16. Hegner, E., H. J.Walter, M. Satir, (1996). Pb–Sr–Nd isotopic compositions and trace element geochemistry of megacrysts and melilitites from the Tertiary Urach volcanic field: Source composition of small volume melts under SW Germany, *Contributions to Mineralogy and Petrology*, v.122 (3), pp. 322–335.
17. Hill, E., B. Wood and J. Blundy (2000). The effect of Ca–Tschermaks component on trace element partitioning between clinopyroxene and silicate melt, *Lithos.*, 53 (3–4), pp. 203–215.
18. Hiroshi, N., H. D. Schreiber, V. M. Richard (1980). Experimental mineral/liquid partition coefficients of

the rare earth elements (REE), Sc and Sr for perovskite, spinel and melilite *Earth and Planetary Science Letters,* v.46, Issue 3 pp.431–437

19. Ivanikov, V. V., A. S Rukhlov, K. Bell, (1998). Magmatic evolution of the melilitite–carbonatite–nephelinite dyke series of the Turiy Peninsula (Kandalaksha Bay, White Sea, Russia), Journal of Petrology., 39 (11–12), pp. 2043–2059.
20. Juk–Pochekutov, K. A., V. C. Gladkich, L. N. Leintiev (1975). Association alkaline basalts Maimacha Kotyi volcano–plutonic formation. Cyrillic. *In book "Petrology and geochemical features ultrabasic and alkaline complex*, M. NAUKA, pp. 50–90.
21. Klemme, S.,S. R. van der Laan, S. F. Foley, D. Günther (1995). Experimentally Determined Trace and Minor Element Partitioning between Clinopyroxene and Carbonatite Melt under Upper–Mantle Conditions, *Earth and Planetary Science Letters*, v.133 (3–4), pp. 439–448
22. Naoki, O., N. Shuji and N. Hiroshi (1981). Mineral/groundmass partition coefficients for nepheline, melilite, clinopyroxene and perovskite in melilite–nepheline basalt, Nyiragongo, Zaire *Geochemical Journal*, v.15, pp.221–228
23. Peterson, T. D. (1989). Peralkaline nephelinites, *Contributions to Mineralogy and Petrology*, v.102, N.3, pp.336–346
24. Petibon, C. M. (1999). The genesis of natrocarbonates: constraints from experimental petrology and trase element partitioning, *A dissertation of Ph.D. of Science. Mernorial University of Newfoundland*, 200 pp.
25. Ramendik, G. I., B. M. Manson, D. A. Turin (1989). Quasi–equilibrium model for the formation of ions in the spark and laser mass spectrometry Cyrillic, *Journal of Analytical Chemistry,* v.44 pp. 996–1007
26. Rass, I. T. (2008). Melilite–bearing and melilite–free rock series in carbonatite complexes: derivatives from separate primitive melts, *Canadian Mineralogist,* v.46, pp.951–969
27. Schairer, I. F., K. Yagi and H. S.Yoder, Jr., (1962). The System Nepheline–Diopside, *Carnegie Inst. Wash. Year Book*, v.61, pp.96–98.
28. Senin, V. G., A. M.Asavin, L. N.Lasutkina, N. V. Korsakova (1989). Measurement Zr and Hf in geological samples by the method of X–ray micro–probe analysis Cyrillic, *Journal of Analytical Chemistry,* № 9.pp. 1671.
29. Shantanu, K., A. Corgne, G. H. Gudfinnsson, M. Bizimis, W. F. Mcdonough and Y. Fei (2005). Kimberlite petrogenesis: Insights from clinopyroxene–melt partitioning experiments at 6GPa in the CaO–MgO–Al_2O_3–SiO_2–CO_2 system *Geochimica et Cosmochimica Acta.*, v.69, No. 11, pp. 2829–2845.
30. Stoppa, F., A. P. Jones, V. V. Sharygin (2009). Nyerereite from carbonatite rocks at Vulture volcano:implications for mantle metasomatism and petrogenesis of alkali carbonate melts, *Cent. Eur. J. Geosci*, v.1 (2) pp.131–151.
31. Sweeney, R. J., V. Prozesky, W. Przybylowicz,. (1995). Selected trace and minor element partitioning between peridotite minerals and carbonatite melts at 18–46 kb pressure, *Geochimica et Cosmochimica Acta,* v.59 (18), pp. 3671–3683.
32. Ulianov, A., O. Muntener, P. Ulmer and P. Thomas (2007). Entrained macrocryst minerals as a Key to the source region of Olivine Nephelinites: Humberg, Kaiserstuhl, Germany, *Journal of Petrology*, v.48, N.6, pp.1079–1118.
33. Wilson, M., J. M. Rosenbaum and E. A. Dunworth (1995). Melilitites: partial melts of the thermal boundary layer? *Contributions to Mineralogy and Petrology*, v.119, N.2–3, pp.181–196.
34. Yoder, H. S. Jr (1967). Akermanite and related melilite–bearing assemblages, *Carnegie Institution of Washington, Yearbook*, v.66, pp.471–477.

Bobrov[1] A. V., Litvin[2] Yu.A., Kuzyura[2] A.V., Dymshits[3] A. M., Jeffries[4] T. Experimental study of partitioning of minor and rare-earth elements between sodium-bearing majoritic garnet and melt at 8.5 GPa

[1] M. V. Lomonosov Moscow State University, Department of Geology, Moscow archi@geol.msu.ru

[2] Institute of Experimental Mineralogy RAS, Chernogolovka

[3] V. I. Vernadsky Institute of Geochemistry and Analytical Chemistry RAS, Moscow

[4] Natural History Museum, London, United Kingdom

This paper summarizes the first results of experimental study of partitioning of minor and rare-earth elements between phases in the system with sodium-bearing (up to 1 wt % Na_2O) majoritic garnet at 8.5 GPa and 1500–1800°C. The studied samples are characterized by significant enrichment of melts in REEs in relation to garnets. All garnets demonstrate increase of the concentrations of HREEs and yttrium, as well as some flattening of partitioning curves with increase of the majoritic component content. Pyroxenes are characterized by much more homogeneous partitioning of minor elements between mineral and melt.

Keywords: [experiment at high temperatures and pressures, sodium-bearing majoritic garnet, partitioning of minor and rare-earth elements between phases]

Reference: Bobrov, A. V., Yu. A. Litvin, A. V. Kuzyura, A. M. Dymshits, T. Jeffries (2012), Experimental study of partitioning of of minor and rare-earth elements between sodium-bearing majoritic garnet and melt at 8.5 GPa, *Vestnik ONZ RAS, 4*

Study of partitioning of minor and rare-earth elements between phases in multi-component and multi-phase mantle matter currently arises significant interest of researchers in relation to the possibility of obtaining of reliable information on the processes of the deep Earth geochemical evolution. A special place among these studies is occupied by experimental investigations at high *PT*-parameters performed for aluminosilicate [*Klemme et al., 2002; Pertermann et al., 2004*], as well as carbonate-silicate diamond-forming [*Kuzyura et al., 2010*] systems with natural chemistry. Studies of intraphase partitioning of minor and rare-earth elements in the mantle magmatic systems with majoritic garnet are very limited [*Draper et al., 2003*], which determined our interest to experimental investigation of these elements in the system with participation of Na-bearing majoritic garnet.

As it was demonstrated in [*Bobrov et al., 2008*], sodium incorporation in majoritic garnet proceeded as the $Na_2MgSi_5O_{12}$ component (so-called sodium majorite Na*Maj*) and was controlled by the three main factors: pressure, temperature, and melt alkalinity. Based on the previously obtained results, we predicted crystallization of garnets with significant sodium concentrations (up to 1 wt % Na_2O) for sodium-rich started compositions (~40–60 mol % Na*Maj*) at a pressure of 8.5 GPa at the solidus of the pyrope (*Prp*)–Na*Maj* system.

Investigations were performed in the Institute of Experimental Mineralogy (Chernogolovka) on a high-pressure toroidal “anvil-with-hole” apparatus using special cell assemblies with graphite heaters [*Bobrov et al., 2008*] at a standardized pressure of 8.5 GPa, within the temperature range of 1500–1800°C. The starting composition $Prp_{50}NaMaj_{50}$ (mol %) was added by the small (2 wt %) controlled portions of minor and rare-earth elements (Li, Rb, Cs, Ba, Th, U, Ta, Nb, La, Ce, Pb, Pr, Sr, Nd, Zr, Hf, Sm, Eu, Gd, Tb, Dy, Y, Ho, Er, Tm, Yb, Lu, Sc, Zn), mainly as oxides. The run duration depended on temperature and ranged from 30 to 90 min.

Within the whole temperature range of T = 1500–1700°C, experimental samples contain the phase association of clinopyroxene + garnet + melt (Fig. 1*a*), which is changed by the two-phase assemblage of garnet + melt with temperature increase (Fig. 1*b*). All garnets are homogeneous and characterized by silicon excess over 3.0 f.u. and admixture of sodium. The maximal content of Na_2O was registered in garnet obtained at 1750°C (Run 2327). The composition of clinopyroxene corresponds to jadeite with a small admixture of enstatite component (up to 4 wt %MgO). Melt is represented by fine-granular quenched aggregate of pyroxene and coesite with a small portion of garnet. The grain sizes in this aggregate slightly varied within the same sample, so that the areas with the smallest grain size were selected for analyses.

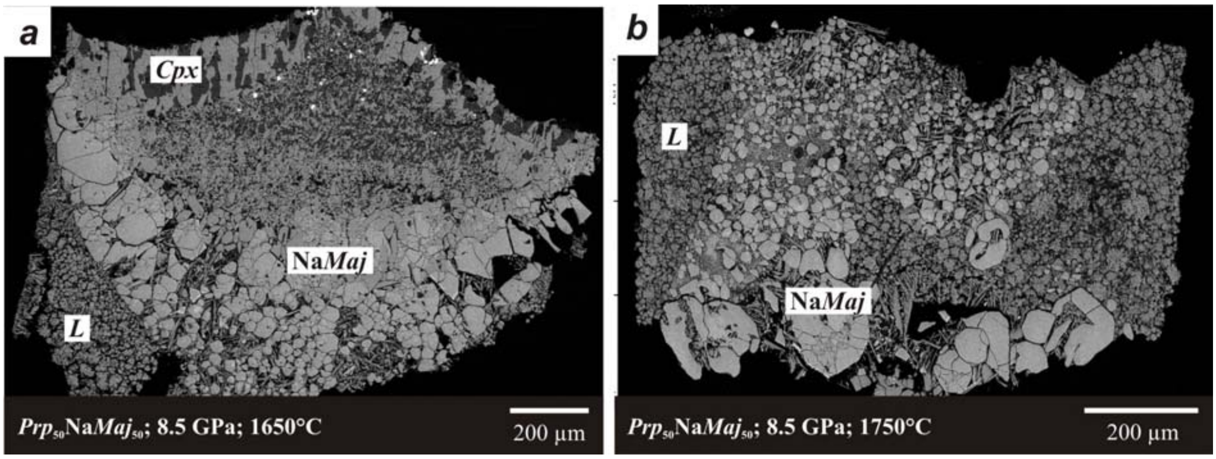

Fig. 1. Back-scattered electron images of textural features of experimental samples obtained in the system $Mg_3Al_2Si_3O_{12}$–$Na_2MgSi_5O_{12}$ at 8.5 ГПа.

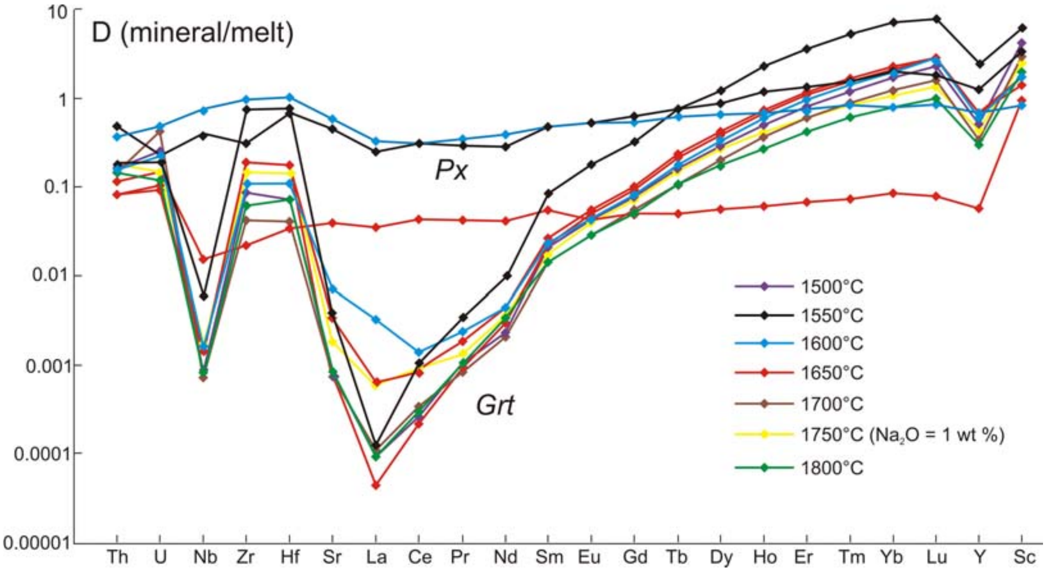

Fig. 2. Partitioning coefficients of minor and rare-earth elements between garnet (*Grt*) and melt and pyroxene (*Px*) and melt in experimental samples depending on temperature.

Samples were investigated on a LA apparatus New Wave UP193FX with ICP-MS Agilent 7500cs in the Laboratory of Analytical Chemistry, Mineralogical Section, Natural History Museum (London, United Kingdom). Synthetic glasses NIST 612 and BCR-2g were applied as standards for calibration of analyses by REEs.

Fig. 2 demonstrates the evolution of partitioning coefficients for minor and rare-earth elements depending on temperature, which, in turn, controls the concentration of sodium in majotitic garnet. The investigated samples are characterized by significant enrichment of melts relatively to garnets in rare-earth elements. Increase of the concentrations of HREEs and Y, as well as some flattening of distribution curves with increase of the concentration of Na-majorite being controlled by the decrease of temperature was observed for all garnets. We should emphasize the higher values of partitioning coefficients for zirconium in comparison with those for hafnium almost for all garnets, except for the most high-temperature ones (1800°C), in which the concentrations of Na_2O do not exceed 0.3–0.4 wt %. Partitioning coefficients for LREEs are comparable with those for less deep garnets. Pyroxenes are characterized by much more homogeneous distribution of minor elements between mineral and melt (Fig. 2).

This study was supported by the Russian Foundation for Basic Research (project nos. 10-05-00654 and 12-05-00426) and by the Foundation of the President of the Russian Federation (grant MD-534.2011.5 for Young Doctors of Sciences and grant NSh-5877.2012.5 for Leading Scientific Schools).

References:

1. Bobrov, A. V., Yu. A. Litvin, L. Bindi, A. M. Dymshits (2008). Phase relations and formation of sodium-rich

majoritic garnet in the system $Mg_3Al_2Si_3O_{12}$–$Na_2MgSi_5O_{12}$ at 7.0 and 8.5 GPa, *Contrib. Mineral. Petrol.,* v. 156, p. 243–257.

2. Draper, D. S., D. Xirouchakis, C.B. Agee (2003). Trace element partitioning between garnet and chondritic melt from 5 to 9 GPa: implications for the onset of the majorite transition in the martian mantle, *Phys. Earth Planet. Inter.,* v. 139, p. 149-169.
3. Klemme, S., J. D. Blundy, B. J. Wood (2002). Experimental constraints on major and trace element partitioning during partial melting of eclogite, *Geochim. Cosmochim. Acta,* v. 66, p. 3109-3123.
4. Kuzyura, A. V., F. Wall, T. Jeffries, Yu. A. Litvin (2010). Partitioning of trace elements between garnet, clinopyroxene and diamond-forming carbonate-silicate melt at 7 GPa, *Mineral. Mag.,* v. 74, p. 227-239.
5. Pertermann, M., M. M. Hirschmann, K. Hametner, D. Gunther, M. W. Schmidt (2004). Experimental determination of trace element partitioning between garnet and silica-rich liquid during anhydrous partial melting of MORB-like eclogite, *Geochem. Geophys. Geosystems,* v. 5, No. 5.

Bukhtiyarov[1] P.G., Persikov.[1] E. S., Newman[2] S.

Experimental study the temperature dependence of water diffusion in dacite melts

[1]Institute of experimental Mineralogy RAS, Chernogolovka, Russia
pavel@iem.ac.ru
[2]California Institute of Technology, Pasadena, USA

The temperature dependence of the diffusion of H2O in haplodacite melts (Ab90Di8Wo2, mole %) has been study at the $P(H_2O)$ = 20MPa in the temperature range of 1000° - 1200°C using a new small gradient methodology. Experimental data obtained is showed that the temperature dependence of water diffusion in haplodacite melts at an average concentration of water C (H_2O) = 0.67 wt. % in them can be described by an exponential Arrhenius-Frenkel's equation, with the activation energy - E = 65 ± 15 kJ / mole.

Key words: [diffusion, temperature, pressure, dacite, model, IR-spectroscopy, water, melts]

Reference: Bukhtiyarov, P. G., E. S. Persikov, S. Newman (2012), Experimental study the temperature dependence of water diffusion in dacite melts, *Vestnik ONZ RAS, 4,*

Knowledge of the temperature dependence of water diffusion in magmatic melts is one of the fundamental problems to understand of a few magmatic processes such as: degassing of magma during volcanic eruptions, the interaction of fluids and magma, the nucleation and growth of crystals and bubbles, and many others. Since the water solubility is much higher than the solubility of other components of the fluid, the diffusion of water is often of the limiting stage of these processes. We have experimentally studied the temperature dependence of the diffusion of H2O in haplodacite melts (Ab90Di8Wo2, mole %) at the $P(H_2O)$ = 20MPa in the temperature range of 1000o - 1200oC using a new small gradient methodology [Persikov *& Bukhtiyarov, 2009; Persikov et. al., 2010*] (see fig.1).

Experiments were performed on a high gas pressure vessel using the original equalizer - separator, that is conduct the experiments in open capsules without of the change of the original geometry of the capsules. Diffusion of water was studied by hydration of anhydrous haplodacite melts, which received by melting of stoichiometric mixtures of the powder of natural mineral (albite + diopside + wollastonite) at the temperature 1500^{o}C for 4 hours in a high temperature furnace at an air atmosphere. Samples pressurized by water in a high gas pressure vessel at the $P(H_2O)$ = 20MPa is heated initially at 1500 ° C / hour to below the required temperature on the 300-500^{o}C, and then very quickly heated to the needed temperature at the rate of 300^{o}C/min. After that melt is kept for the time which is need to form of the diffusion profile in the melt and spent the isobaric quenching at 300 - 500 ^{o}C/min. Concentration of water along the diffusion profiles were determined by quantitative FTIR spectroscopy using of the Beer-Lambert's equation. The diffusion of water was determined by analytical [*Crank, 1975*] and numerical solutions to solve of the second Fick's law of diffusion.

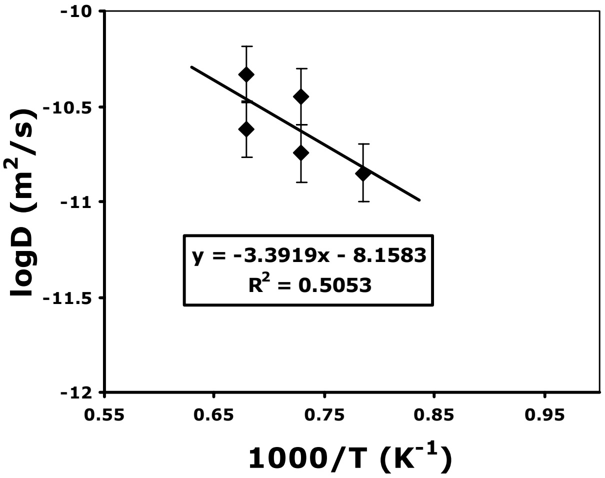

Fig.1. The temperature dependence of water diffusion in haplodacite melts ($C(H_2O)$ = 0.67 wt.%): ◆ – experimental data with the standard deviation ± 30 % rel.

Analysis of experimental data showed that the temperature dependence of water diffusion in haplodacite melts at an average concentration of water C (H_2O) = 0.67 wt. % in them can be described by the following exponential Arrhenius- Frenkel's - equation:

$$D = D_0 \bullet \exp(-E/RT) \qquad (1),$$

where R = 8.314 J/mole·K is the universal gas constant, E is the activation energy of water diffusion for haplodacite melts (J/mole), and T is in K. The activation energy obtained for the activation energy of water diffusion in haplodacite melts ($C(H_2O)$ = 0.67 wt.%) – E = 65 ± 15 kJ / mole) is well consist to a previously obtained data for the polymerized haplogranitic melts ($C(H_2O)$ = 0.5 wt.%) – E = 64 ± 10 kJ / mole [*Nowak & Behrens, 1997*] and for the obsidian melts ($C(H_2O)$ = 0.5 wt.%) – E = 67 ± 21 kJ / mole [*Shaw, 1973*]. But it is quite different with the values of the activation energy of water diffusion in natural potassic melts ($C(H_2O)$ = 0.5 wt.%) - E = 147 ± 42 kJ / mole [*Freda et al. 2003*] and in basalt melts ($C(H_2O)$ = 0.2 wt.%) – E = 126 ± 32 kJ / mole [*Zhang Y. & Stolper, 1991*]. It should be noted that such comparing of activation energy of water diffusion in the melts of different composition is rightfully in strict meaning if the value of D_0 in the equation (1) is a constant.

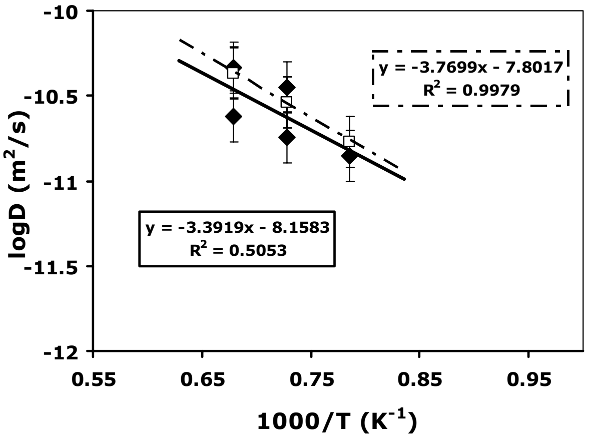

Fig. 2. Temperature dependence of water diffusion in haplodacite melts ($C(H_2O) = 0.67$ wt.%) (dark symbols - an experimental data, open symbols - predicting data which were obtained using a new model; [*Persikov et al., 2010*]).

This problem is solved now for the calculation of activation energy of viscous flow [*Persikov, 1991, 1998*] but it is not solved for the calculation of activation energy of water diffusion in the melts of different composition. Therefore we are suggested of the next way to solve of this problem. Recently a new model was proposed to calculate the water diffusion in a wide range of composition of magmatic melts, pressures and temperatures [*Persikov et al., 2010*]. The predicted temperature dependence of water diffusion in haplodacite melts have been obtained using this model (see fig. 2). The data on the fig. 2 shows of a good agreement between experimental and predicted values of the temperature dependence of water diffusion in haplodacite melts with standard deviation which is equal ± 0.15 log of $D(H_2O)$. Predicted value obtained for the activation energy of water diffusion in haplodacite melts ($C(H_2O) = 0.67$ wt.%) – E = 64 ± 5 kJ / mole is practically the same to the experimental value.

Conclusions:

1. A new experimental data is indicates that the temperature dependence of water diffusion in haplodacite melts with an average concentration of water in melt C (H_2O) = 0.67 wt. % and in the temperature range of 1000° - 1200°C is obey the exponential Arrhenius-Frenkel's equation with an activation energy equals E = 65 ± 15 kJ / mole.

2. Model developed to calculate of the water diffusion in silicate melts [*Persikov et al., 2010*] is allowed to obtain of a well enough data on temperature dependencies of water diffusion in magmatic melts.

We thank E.M. Stolper for his helpful discussions.

This work was supported by RFBR, grant No 12-05-00164 and by DES, program No 9

References:

1. Crank, J. (1975). The mathematics of diffusion, Clarendon Press, Oxford, 414 p.
2. Nowak, M., H. Behrens (1997). An experimental investigation on diffusion of water in haplogranitic melts, *Contrib. Mineral. Petrol.,* v. 126, pp. 365–376.
3. Shaw, H. R. (1997). Diffusion of H_2O in granitic liquids; Part I. Experimental data; Part II. Mass transfer in magma chambers, *In: "Geochemical Transport and Kinetics*" A. W. Hofmann et al., Eds. Carnegie Institute Washington Publ., Washington, v. 634, pp. 139–170.
4. Freda, C., D. R. Baker, C. Romano, P. Scarlato (2003). Water diffusion in natural potassic melts, In: *Volcanic Degassing., Geol.Soc. London Special Publication, 213,* Oppenheimer, C., Pyle, D.M., Barclay, J. (Eds.), London Geological Society, pp. 52–62.
5. Zhang, Y., E. M. Stolper (1991). Water diffusion in a basaltic melt, *Nature,* v. 351, pp. 306–309.
6. Persikov, E. S., P. G. Bukhtiyarov (2009). Interrelated structural chemical model to predict and caculate viscosity of magmatic melts and water diffusion in a wide range of compositions and T-P parameters of the Earth's crust and upper mantle, *Russian Geology and Geophysics,* v. 50, № 12, pp. 1079–1090.
7. Persikov, E. S., S. Newman, P. G. Bukhtiyarov, A. N. Nekrasov, E. M. Stolper (2010). Experimental study of water diffusion in haplobasaltic and haploandesitic melts, *Chemical Geology,* v. 276, pp. 241–256.
8. Persikov, E. S. (1991). The viscosity of magmatic liquids: experiment, generalized patterns. A model for calculation and prediction. Applications, *In: Physical chemistry of magmas. Advances in Physical Geochemistry.* L. L. Perchuk & I. Kushiro Eds., Springer-Verlag, New York, v. 9, pp. 1–40.
9. Persikov, E. S. (1998). The viscosity of model and magmatic melts under *P,T* - parameters of the Earth's crust and upper mantle, *Russian Geology and Geophysics,* v. 39, pp. 1780–1792.

Volovetskii [1]M. V., Lukanin [1]O. A., Rusakov [2] V. S. Structural state of iron ions in the glasses of granitoid composition synthesized at various T-fO_2 conditions

[1]Vernadsky Institute of Geochemistry and Analytical Chemistry of the RAS, Moscow lukanin@geokhi.ru

[2]Faculty of Physics of the Moscow State University, Moscow *mih_volov@mail.ru;*

Mössbauer study of the experimental glasses of granitic and pantelleritic compositions obtained by quenching of melts exposed at various *T–f*O_2 conditions (1200–1420°C, 10^{-12}–$10^{-0.7}$ bar) showed that Fe^{2+} ions are distributed mainly on the octahedral (and/or five-coordinated) positions, regardless of the Fe^{3+}/Fe^{2+} in the melt (glass), and play the role of modifier cation. Coordination of Fe^{3+} ions depends on the degree of oxidation of the iron atoms. With increasing fraction of ferric iron, its coordination changes from octahedral to tetrahedral. Thus, being a network-modifying cation under reducing conditions, Fe^{3+} becomes predominantly a network-former under oxidizing conditions. The structural role of Fe^{2+} as network-modifying cations does not change fundamentally with variations in the degree of iron oxidation. The change of Fe^{3+} coordination in aluminosilicate melts of various compositions occurs at similar values of $Fe^{3+}/\Sigma Fe \geq 0.5$.

Key words: I[ron ions, structural state, silicic aluminosilicate melts, glasses, Mössbauer spectroscopy]

Reference: Volovetskii, M. V., O. A. Lukanin, V. S. Rusakov (2012), Structural state of iron ions in the glasses of granitoid composition synthesized at various T-fO_2 conditions, *Bulletin of the Department of Earth Sciences*, 4, (doi: ...)

The structural state of iron ions was studied by Mössbauer spectroscopy in glasses quenched from natural silicic aluminosilicate melts of granite (I2) and pantellerite (P9) compositions exposed to various *T–f*O_2 (1100–1420°C, 10^{-12}–$10^{0.68}$ bars) conditions at a total pressure of 1 atm. [*Volovetskii et al, 2012*]. Processing and analysis of the Mössbauer spectra included the reproduction of two independent distributions p(ε) of quadrupole splitting, ε, corresponding to Fe^{3+} and Fe^{2+}, because this parameter is the hyperfine interaction is most sensitive to the geometry of the surrounding. The linear correlation of parameters was taken into account for the distribution function of the hyperfine parameters Fe^{2+}: the quadrupole splitting (ε) and the Mossbauer isomer shift (δ) [*Rusakov, 1999, 2000*]. The crystal-chemical identification of partial Mössbauer spectra was performed by comparing the obtained isomer shifts, δ, for ^{57}Fe nuclei in the samples with the results of the Mossbauer and X-ray investigation of a large set of crystal phases of various mineral systems [*Menil. 1985; McCammon, 1995*]. The rate of structural equilibration in melt is much higher than that of melt–gas (air furnace) equilibration. This allowed us to use some glasses obtained under nonequilibrium conditions for the assesment of the influence of the degree of iron oxidation on its structural state in melts.

Fig. 1 shown the Mössbauer hyperfine parameters, quadrupole splitting (ε) and isomer shift (δ), of the synthetic quenched glasses, which can be used for the estimation of the structural state of iron ions. Also shown are the ranges of isomer shifts typical of oxygen environments of iron in different valence state in crystalline materials (octahedral, five-coordinated, and tetrahedral). It should be noted that the range of five-coordinated Fe overlaps with the ranges of octahedral and, to same extent, tetrahedral positions; therefore the range of δ corresponding to the five-fold coordination cannot be distinguished.

The ε and δ values of Fe^{2+} in the two series of quenched glasses, I2 and P9, vary in a narrow ranges (Fig.1) and do not change significantly depending on fO_2 and *T*. The isomer shift values correspond mainly to six- and five-coordinated Fe^{2+}. Much more significant variation were observed for the parameters of Fe^{3+}. The quadrupole splitting for Fe^{3+} in the series I2 glasses are, in general, approximately 0.2 mm/s higher than those in the series P9 glasses, which could be related to a more heterogeneous local environment of Fe^{3+} in the granitic glasses (Fig.2).

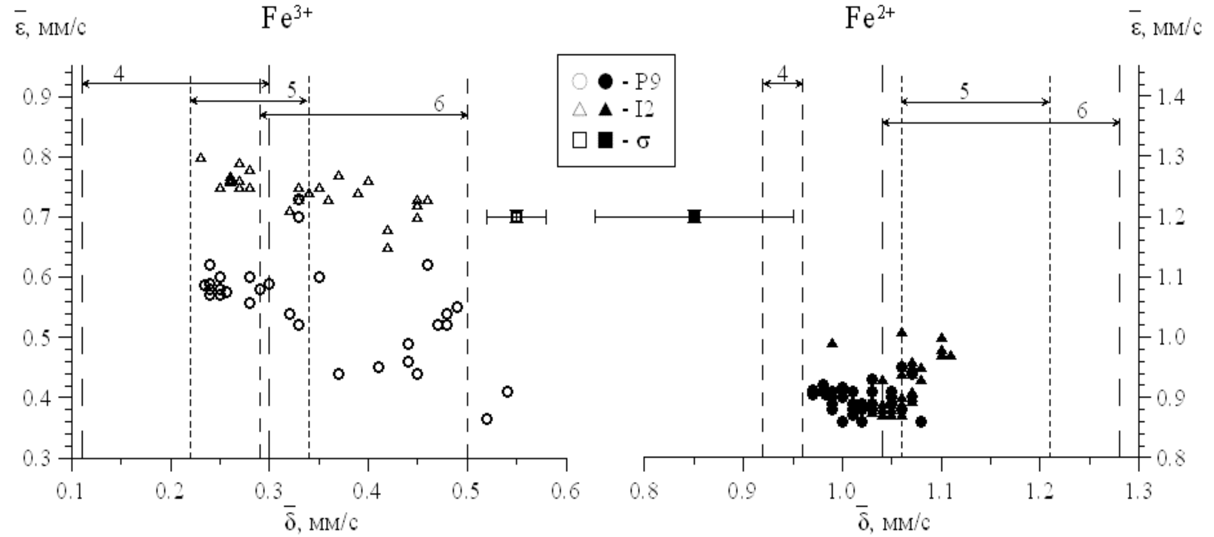

Fig.1. Hyperfine parameters of the partial spectra of Fe^{3+} and Fe^{2+} in the δ–ε coordinates. The maximum standard deviations of the parameters of Fe^{3+} and Fe^{3+} are shown in the diagram.

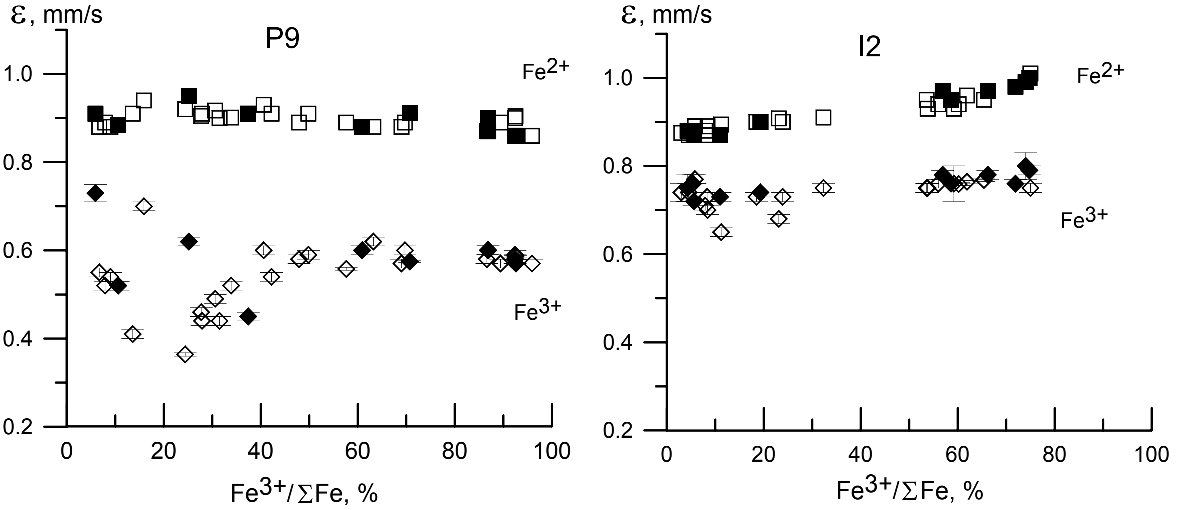

Fig.2. The dependence of the Mössbauer quadrupole splitting for Fe^{2+} and Fe^{3+} on the oxidation state of iron in granitic (I2) and pantelleritic (P9) glasses. Filled symbols – samples are closest to equilibrium with the atmosphere furnace at a temperature of the experiment.

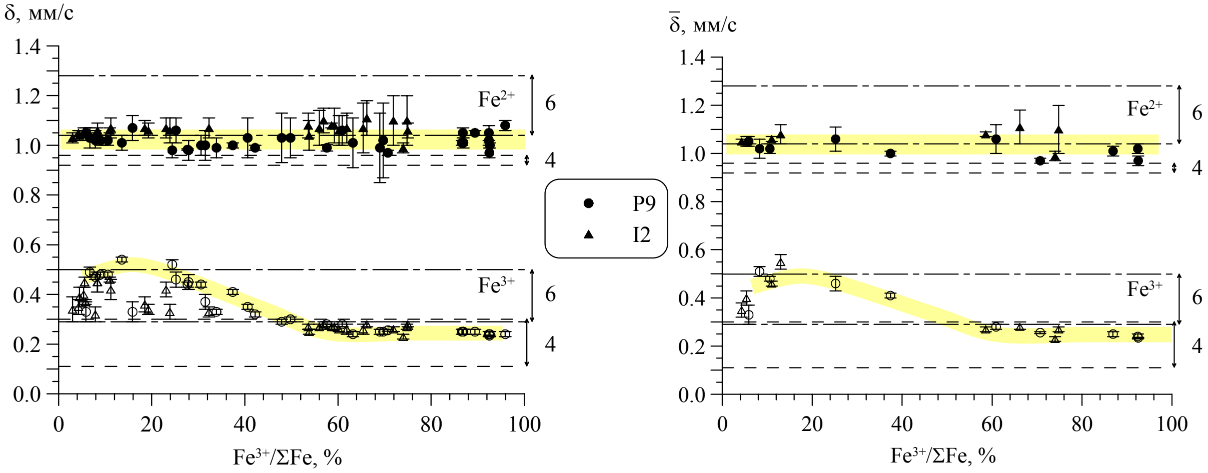

Fig.3. Dependence of the Mossbauer isomer shift for Fe^{2+} and Fe^{3+} on the degree of iron oxidation: for all samples (*left*) and for samples with the equilibrium redox state of iron (*right*)

The wide range of variations in the isomer shift for Fe^{3+} in both glass series is evidently related to a change its structural positions in melts under various redox conditions. Figure 3 shows the dependence of the Mössbauer isomer shift, δ, on the degree of iron oxidation, i.e., the content of Fe^{3+} relative to total iron in the glass. Also shown are the ranges of isomer shift typical of octahedron and tetrahedron oxygen environments of iron in different valence states in crystalline phases. In the glasses of both series, the isomer shift for Fe^{3+} increases gradually with increasing degree of iron oxidation and passes gradually, when Fe^{3+} fraction decreases below 50–45 %, from the range characteristic of octahedral oxygen environments to the range of value corresponding to tetrahedral coordination. Hence, with increasing fraction of ferric iron, its coordination changes from octahedral to tetrahedral. Degree of iron oxidation does not affect significantly the isomer shift for Fe^{2+} in the glasses of both series; its values lie within a narrow range near the lower boundary of intervals characteristic of octahedral and five-coordinated positions (Fig.3).

It can be noted that the value of isomer shifts for series P9 are slightly lower (by approximately 0.05 mm/s) than those for I2, which may indicate a difference in the local environment of Fe^{2+} and/or some variations in the length of Fe^{2+}–O bonds.

The Mossbauer investigation of quenched granitic and pantelleritic glasses with different degrees of iron oxidation supported the previously observed phenomenon of a change in the dominant coordination of Fe^{3+} in natural and synthetic aluminosilicate melts from octahedral to tetrahedral with increasing degree of iron oxidation [*Mysen, 1988*]. Thus, being a network-modifying cation under reducing conditions, Fe^{3+} becomes predominantly a network-former under oxidizing conditions. The structural role of Fe^{2+} as network-modifying cations does not change fundamentally with variations in the degree of iron oxidation. The change of Fe^{3+} coordination in aluminosilicate melts of various compositions occurs at similar values of $Fe^{3+}/\Sigma Fe \geq 0.5$. For the I2 and P9 melts at temperatures of 1320–1420°C, this corresponds to fO$_2$ values higher than 10^{-5}–10^{-3} (2–3 log units above FMQ).

This work was supported by RFBR (grants 08-05-00022, 11-05-00926).

References :

1. Volovetskii M. V., O. A. Lukanin, V. S. Rusakov, and A. A. Kargal'tsev (2012). Influence of oxygen fugacity and temperature on the redox state of iron in natural silicic aluminosilicate melts, *Geochemistry International,* v. 50, No. 4, pp. 330–343.
2. Rusakov, V. S. (1999). Restoration of the distribution functions of hyperfine parameters of Mössbauer spectra of locally inhomogeneous systems, *Proceedings of the Academy of Sciences, Ser. Physical.* v. 63, No 7, pp. 1389–1396 (In Russ).
3. Rusakov, V. S. (2000). Mössbauer spectroscopy of locally inhomogeneous systems. *Almaty*, p.431 (In Russ).
4. Menil, F. (1985). Systematic trends of the ^{57}Fe Mössbauer isomer shifts in (FeO$_n$) and (FeF$_n$) polyhedra, *J. Phys. Chem. Solid,*. v. 46, pp. 763–789.
5. McCammon, C. (1995). Mössbauer spectroscopy of minerals, *Mineral Physics and Crystllography. A Handbook of physical Constants. AGU Reference Shelf 2.*
6. Mysen B.O. (1988). Structure and properties of silicate melts. Elsevier. Amsterdam, p. 354.

Gorbachev[1] N. S., Ravna [2]E., Nekrasov[1] A.N., Kullerud[2] K. Phase relationship and geochemistry of garnet-bearing carbonatites of Trosø area, Norway

[1]Institute of experimental mineralogy RAS, Chernogolovka
gor@iem.ac.ru
[2]University Tromsø, Norway

The phase composition and geochemistry of garnet-containing carbonatites UHPC Tromsø area studied. The matrix of UHPC calcite-dolomite composition contains inclusions of garnet, and accessory minerals - apatite, sphene, ilmenite, rutile. There are three generation of garnet: Grt1, depleted in REE (<2.10^{-2} wt.%); Grt2-3, anomalously enriched (up to 4-8 wt.%) in LREE. Carbonate C and silicate Si fractions of UHPC differ on concentration of trace elements. Anomalous REE distribution in UHPC indicates a lack of equilibrium between Grt and carbonatite melt.

Keywords: [carbonatite, high pressures, phase composition, geochemistry, experiment]

Reference: Gorbachev, N.S., E. Ravna , A.N. Nekrasov., K. Kullerud (2012), Phase relationship and geochemistry of garnet-

bearing carbonatites of Trosø area, Norway, *Vestnik ONZ RAS, 4,* (doi:)

In connection with the problem of the existence of carbonate magmas in the upper mantle studied the phase relations and geochemistry of garnet-bearing ultra-high pressure carbonatites (UHPC) Tromsø area, Norway. The matrix of UHPC is represented by carbonate C calcite-dolomite composition with inclusions of garnet Grt and accessory minerals - apatite, sphene, ilmenite, rutile. The samples were studied by microprobe, trace elements were determined by ICP MS.

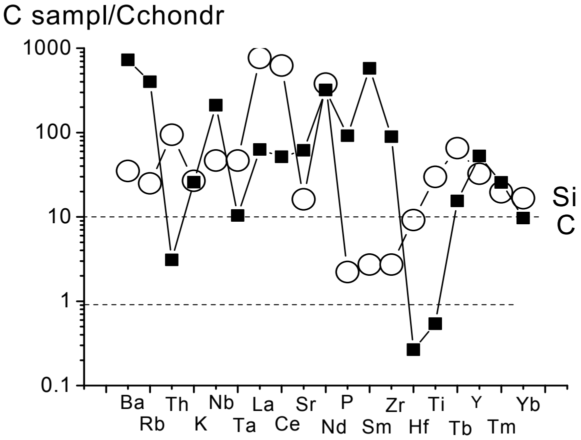

Fig. 1. Normalize for chondrite concentration of trace elements in carbonate C and silicate Si fractions of UHPC

On structure and composition it is allocated three generation of Grt: early, Grt1, of pyr15-gros25-alm60 composition, depleted in REE ($<2.10^{-2}$ wt.%); reacting Grt2-3 of pyr5-gros65-alm30 composition, anomalously enriched (up to 4-8 wt.%) in LREE .

The abundances of trace elements in the UHPC, its carbonate C and silicate Si fraction were examination. Compared to silicate, carbonate fraction is enriched in Ba, Rb, Nb, Sr, P, Zr, depleted in Hf, Ti, Th, Ta (fig. 1).

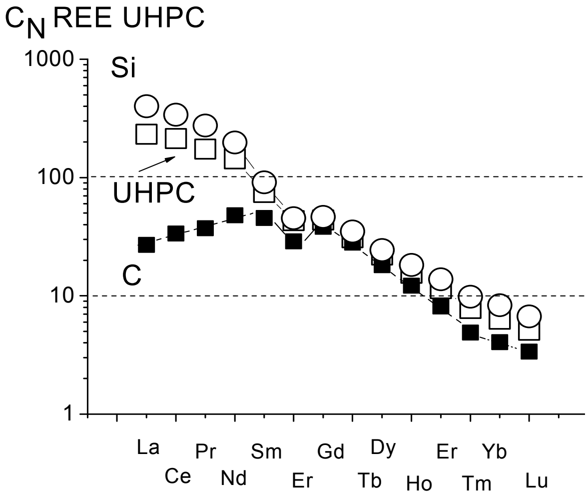

Fig. 2. Normalize for chondrite concentration of REE in UHPC, its carbonate C and silicate Si fractions

Carbonate and silicate fraction of UHPC differ in REE concentrations and the character of its dependence from atomic number N REE. Silicate fraction enriched in REE, the dependence of the normalized for chondrite REE concentrations C_N from N REE has negative slope with slight Eu minimum. In the carbonate fraction to the dependence of C_N-N REE has an extreme character with maximum at Gd-Tb. The largest differences are observed in the distribution of LREE. In the silicate fraction C_N REE reduced from 500 at La to 50 for Sm, in carbonate fraction C_N REE rise from 30 to 45 at La to Sm. Starting from Gd to Lu REE behavior is similar in silicate fraction C_N REE reduced to 8, and in carbonate C fraction up to 5 (fig. 2).

Since the silicate fraction to UHPC dominates Grt, then we can assume that D REE - partition coefficients between silicate and carbonate fraction to characterize the partition coefficients REE between Grt and carbonatite melt C. However, D REE Si/C~D REE Grt/C in the UHPC differ from the experimental D Grt/C. In UHPC dependence of D REE Si/C is an extreme character, decreasing from 18 to 1.2 for La to Gd-Tb, and then increasing to 2 at Tm-Lu. According to our experimental data, the dependence of D REE Grt / C is positive, increasing from 0.07 at La to 10 at Lu (fig. 3).

Anomalous REE distribution in UHPC indicates a lack of equilibrium between Grt and carbonatite melt at formation of carbonatite melt at melting of upper mantle.

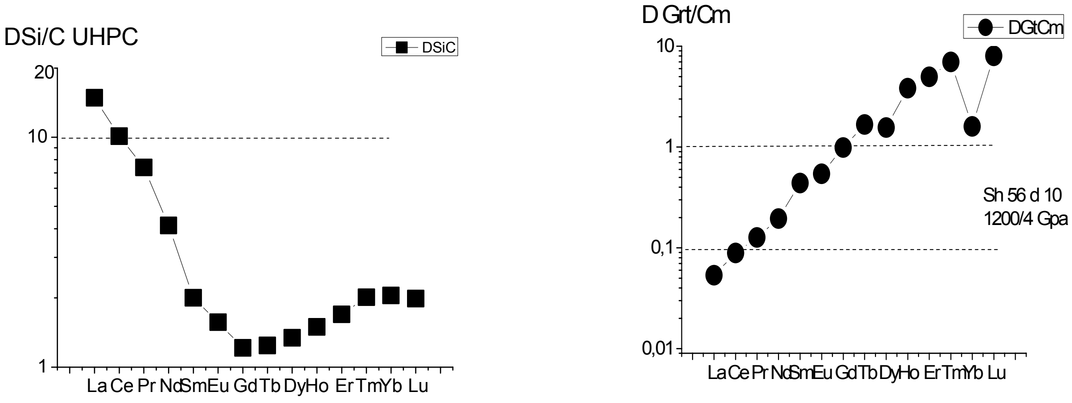

Fig. 3. Partition coefficients REE between silicate and carbonate fraction of UHPC (D REE Si/C) and partition coefficients REE between Grt and carbonatite melt (D REE Grt/Cm) (for our experimental datas)

Supported by grant RFBR 09-05-0113-a, 12-05-00777-a

Gorbachev N.S., Nekrasov A.N., Kostyuk A.V., Sultanov D.M. Experimental study melting of garnet-bearing carbonatite

Institute of experimental mineralogy RAS gor@iem.ac.ru.

Melting of garnet-bearing carbonatite studied at T=950–1450ºC, P=3.8–4.0 Gpa. Temperature "dry" liquidus is ~ 1270ºC, "dry" solidus is ~ 1150ºC. It have the full miscibility between silicate and carbonate melts. In experiments with H_2O+CO_2 fluid at T=1450ºC, P=4 GPa stratification of carbonatite melt on highly and low-carbonate-silicate liquids with graphite allocation was observed. At melting UHPC with H_2O+CO_2 fluid T liquidus goes down to T ~ 1250ºC, T solidus - up to ~ 950ºC. In subliqudus areas with carbonatite melt zonality garnet co-exists

Key word: [carbonatite, experiment, melting, high pressure, melt, phase composition]

Reference: Gorbachev, N. S., A. N. Nekrasov, A. V. Kostyuk, D. M. Sultanov (2012), Experimental study melting of garnet-bearing carbonatite, *Vestnik ONZ RAS*, 4, (doi:)

Introduction In connection with the problem of the genesis of carbonatites at T-P of upper mantle (950–1450 º C, 3.8–4.0 GPa) studied the melting of garnet-bearing ultra-high pressure carbonatite UHPC Tromsø area, Norway in "dry" conditions and with $H_2O + CO_2$ fluid.

Experimental method Experiments were carried out in the IEM RAS on the "anvil with hole" in Au and Fe-bearing platinum capsules using a quenching technique. The temperature is measured by a Pt30Rh/Pt6/Rh thermocouple. At high temperature, pressure is calibrated using a curve of balance quartz - coesite. Uncertainties are ± 10ºC for temperature and ± 0.1 GPa for pressure measurements. Duration of experiments were from 6 to 18 hours. Products of experiments were studied by

PC-controlled scanning electron microscope Tescan VEGA TS 5130MM with detector of secondary and backscattered electron on the YAG-crystals and energy dispersive X-ray microanalyzer with semi-conductor Si(Li) detector INCA Energy 350.

Results Temperature T "dry" liquidus UHPC ~ 1270 ºC. It is established full miscibility between silicate and carbonate melts. At quenching carbonatite melt the mix of microlites of variable composition, from the carbonate-silicate to silicate-carbonate is formed.

In the range of T 1250–1200ºC with carbonatite melt garnet Grt co-exists. This garnet differing from initial garnet UHPC by absence of zonality, higher content of CaO, TiO_2, lower Al_2O_3, FeO.

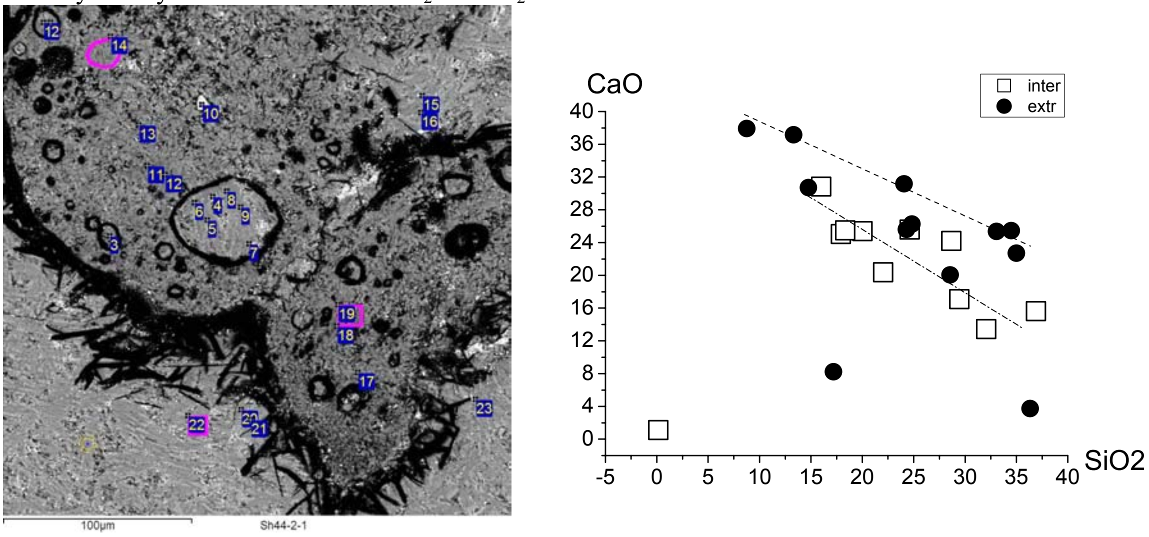

Fig. 1. Stratification carbonatite melt on highly and low- carbonate-silicate liquids with graphite allocation: microphoto an composition of the quenching carbonatite melt sample. 1450ºC, 4 GPa

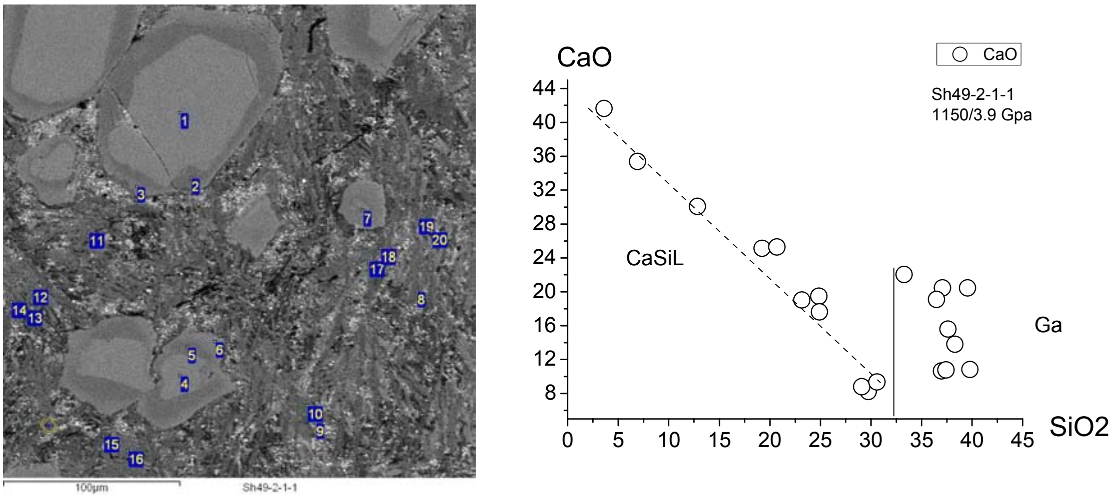

Fig. 2. Microphoto and composition of the quenching sample with zonality garnet. T 1150ºC, P=4 GPa

Temperature "dry" solidus is ~1150ºC. In the range T from 1150 to 950ºC near soliduse and subsolidus associations are presented calcite Cc, garnet Grt, clinopyroxene Cpx, flogopite Flog and accessory minerals – apatite Apt, ilmenite Ilm, rutile Rt.

In experiments with H_2O+CO_2 fluid temperature liquidus goes down to 1250ºC. At T=1450ºC, P=4 GPa stratification carbonatite melt on highly and low-carbonate-silicate liquids with graphite allocation was observed (fig. 1).

In range T=1250–1150ºC with carbonatite melt the zonality garnet co-exists. Its reactionary border in comparison with its central part is enriched in FeO, MgO, MnO and depleted in. CaO, TiO_2, SrO (fig. 2).

Zonality of garnet testifies to interaction of carbonatite melt with garnet at which the reactionary garnet is enriched in CaO, TiO_2, SrO.

At melting of UHPC with H_2O+CO_2 a fluid temperature solidus goes down to T ~ 950ºC. At T=950ºC, P=3.8 GPa carbonatite melt co-exists with Cc, Flog, Grt, Cpx, Apt. At increase T up to 1050ºC the portion of carbonatite melt increases, disappears Cpx, on liqudus present Cc, zonality Grt, Flog,

Results of experiments testify to formation characteristic for UHPC associations a carbonate-zonality garnet in the range of T =1150-1250ºC.

Supported by grant RFBR 09-05-0113-a, 12-05-00777-a.

Gorbachev N.S., Kostyuk A.V., Nekrasov A.N., Sultanov D.M. Experimental study distribution of trace elements between clinopyroxene, garnet and silicate melts

Institute of experimental mineralogy RAS gor@iem.ac.ru.

Distribution of 25 trace elements between Cpx, Grt, and silicate melts experimentally studied. There were wide variations (from n10^{-3} to 10 and over) in the partition coefficients rare elements between Cpx, Grt, silicate melts – D Cpx, Grt/m. Elements, preferably distributed in the Grt–Cpx restite (HREE, Y, V with DGrt, Cpx/m> 1) are compatible. The behavior of LILE, HFSE elements - Li, Be, Ba, Th, Ti, Zn, U, Nb, Ta, Pb, Hf, LREE is similar to the behavior of incompatible elements, it is preferable to be distributed in the melt, DGrt, Cpx/m <1. All rare e elements mostly concentrated in the alkaline silicate melt, D Cpx/m of these elements <1.

Keywords: [experiment, high pressures, rare elements, garnet, clinopyroxene, melt]

Reference: Gorbachev, N.S., A.V. Kostyuk, A.N. Nekrasov, D.M. Sultanov (2012), Experimental study distribution of trace elements between clinopyroxene, garnet and silicate melts, *Vestnik ONZ RAS*, 4, (doi:)

Partial melting of eclogite were studied at T = 1400ºC, P= 4 GPa at "dry" condition and with alcalic-carbonaceous fluid. At partial melting “dry” eclogite with clinopyroxene Cpx and garnet Grt coexist melts of andesite-dacite composition. At melting of eclogite with alcalic-carbonaceous fluid Cpx coexist with fluid-bearing alkaline silicate melt. To elucidate the behavior of trace elements during metasomatism and melting of eclogites experimentally studied distribution of 25 trace elements between Cpx, Grt, and acidy and alcaline silicate melt.

Experiments were carried out in the IEM RAS on the "anvil with hole" in Au and Fe-bearing platinum capsules using a quenching technique. The temperature is measured by a Pt30Rh/Pt6/Rh thermocouple. At high temperature, pressure is calibrated using a curve of balance quartz–coesite. Uncertainties are ± 10ºC for temperature and ± 0.1 GPa for pressure measurements. Duration of experiments were from 6 to 18 hours. Products of experiments were studied by PC-controlled scanning electron microscope Tescan VEGA TS 5130MM with detector of secondary and backscattered electron on the YAG-crystals and energy dispersive X-ray microanalyzer with semi-conductor Si(Li) detector INCA Energy 350.

There were wide variations in the partition coefficients rare elements between Cpx, Grt, silicate melts m D Cpx, Grt / m from n10-3 to 10 and over (fig. 1).

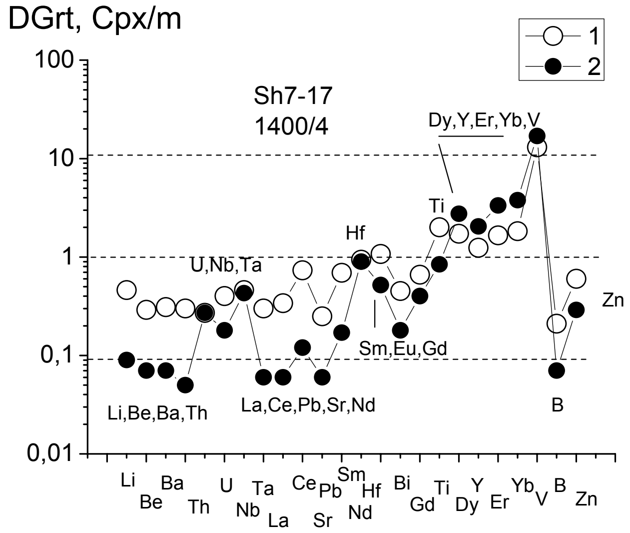

Fig. 1. Partition coefficients rare elements between Cpx, Grt, and andesite-dacite silicate melts. 1 – D Cpx/m, 2 – D Grt/m. T = 1400ºC, P = 4 GPa

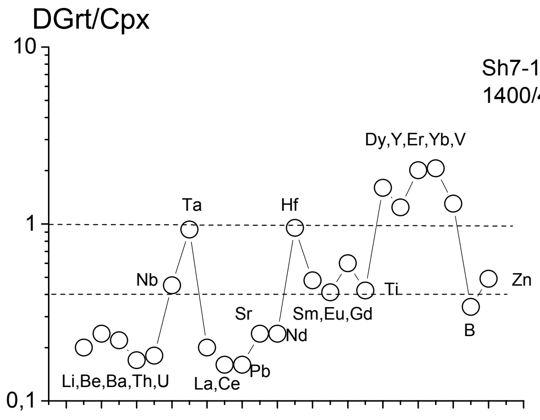

Fig. 2. Partition coefficients rare elements between Grt and Cpx, in equlibrium wth andesite-dacite silicate melts. T = 1400ºC, P = 4 GPa

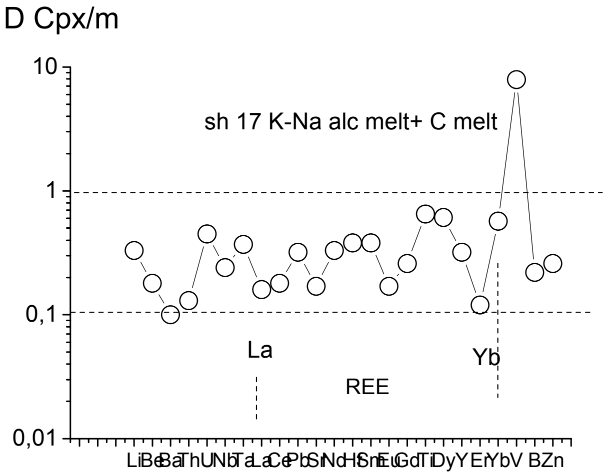

Fig. 3. Partition coefficients rare elements between Cpx and alkaline melt

By analogy with the peridotite system elements, preferably distributed in the Grt–Cpx restite (HREE, Y, V with partial coefficient DGrt, Cpx/m> 1) are compatible. The behavior of LILE, HFSE elements – Li, Be, Ba, Th, Ti, Zn, U, Nb, Ta, Pb, Hf, LREE is similar to the behavior of incompatible elements, it is preferable to be distributed in the melt, DGrt, Cpx / m <1 .For the association of Grt-Cpx incompatible elements are preferably distributed in the Cpx, compatible – HREE, Y, V – in Grt (fig. 2).

In case of partial melting of eclogite from the alkaline aqueous fluid with alkaline carbonate melt m coexisting Cpx.. With the exception of V, elements of LILE, HFSE, REE, siderophyle mostly concentrated in the silicate melt, D Cpx / m of these elements <1 (fig. 3).

Wide variations in D Cpx, Grt / m rare elements indicates a significant fractionation of trace elements during partial melting of eclogite at “dry” conditions. These results show, that alkaline melts are efficient concentrator of trace elements and can play important role in enrichment of mantle at mantle metasomatose.

Supported by grant RFBR 09-05-0113-a, 12-05-00777-a.

Zaitsev V.A., Senin V.G. Oxiftoride srontioperovskite $(Sr_{1-x}Na_x)TiO_{3-x}F_x$ – the synthetic analogue of tausonite

V. I. Vernadsky Institute of Geochemistry and Analytical Chemistry RAS, Moscow alkaline@geokhi.ru

$NaTiO_2F$ component of perovkite-structure solid solution was detected in synthetic analog of tausonite (srontioperovskite), formed as the product of incongruent melting of lamprophyllite and Ba-rich lamprophyllite. It was concluded that perovskite-type minerals may be significant bearier of fluorine in mantle.

Key words: experiment, perovskite solid solution, anion isomorphism, tausonite

Reference: Zaitsev, V. A., V. G. Senin (2012), Oxiftoride srontioperovskite $(Sr_{1-x}Na_x)TiO_{3-x}F_x$ – the synthetic analogue of tausonite, *Vestnik ONZ RAS, 4,*

The tausonite ($SrTiO_3$) is a member of perovskite group. It was discovered in ultraagpaitic rocks of Murun massif as brown isometric crystals up to 5 mm. [*Vorobev et al., 1984*]. The main admixtures are Ca(0.8–0.16 a.p.f.u), Na (0.05–0.2 a.p.f.u), REE (up to 0.2 a.p.f.u) and Nb up to (0.01 a.p.f.u) [*Vorobev et al., 1984*] .

Sodium-bearing synthetic analogue of tausonite was having been reported as the product of incongruent melting of lamprophyllite and Ba-rich lamprophyllite. It also was crystallized form titanosilicate melt in lamprophyllite-nepheline phase diagram. The stability field of this phase occupy the high-temperature part of the diagram [*Zatsev et al, 2004 a,b*]

Like the natural tausonite, synthetic analogue usually forms cubic crystals or fluorite-law twins. The composition of tausonite from Murun massif can be described as a mixcure of tausonite ($SrTiO_3$), loparite ($Na_{0.5}REE_{0.5}TiO_3$) and lueshite $NaNbO_3$ minals. There are two charge compensation mechanism for incorporation Na^+ instead Me^{2+} in natural perovkite-type minerals: $Me^{2+} + Ti^{4+} \rightarrow Na^+ + Nb^{5+}$- and $2Me^{2+} \rightarrow Na^+ + REE^{3+}$. The synthetic tausonite contain high concentration of Na (up to 0.2 a.p.f.u) but low concentration of Nb (<0.05 a.p.f.u) and REE (was not included to the system). It was supposed that electric charge compensated by the anion vacancies. For description of sodium-bearing tausonite chemistry were suggested formula $(Sr_{1-x}Na_x)TiO_{3-x/2}$ and hypotetical minal $NaTiO_{2.5}$ [*Zatsev et al, 2003, Zatsev et al, 2006*].

Table. Composition of syntetic sodium-bearing tausonite

Electron-microprobe analyses %															
Шихта	T°C	Na_2O	MgO	Al_2O_3	SiO_2	K_2O	CaO	TiO_2	MnO	FeO	SrO	Nb_2O_5	BaO	F	Сумма	-O=F_2
3Lam:1Ne	812	2.06	0.02	0.29	1.63	0.01	1.94	42.02	0.29	0.26	49.15	0.72	0.33	1.10	98.72	98.26
3Lam:1Ne	812	2.10	0.02	0.36	1.28	0.01	1.93	43.22	0.30	0.13	49.94	0.76	0.31	1.43	100.36	99.76
3Lam:1Ne	827	1.28	0.00	0.03	0.00	0.01	1.75	45.64	0.07	0.12	50.38	1.03	0.13	0.25	100.44	100.33
3Lam:1Ne	827	1.43	0.02	0.08	0.11	0.00	1.78	45.30	0.04	0.21	48.88	1.02	0.18	0.08	99.05	99.02
15Lam:8Ne	812	1.45	0.02	0.08	0.21	0.02	1.74	42.94	0.19	0.26	50.12	1.08	0.31	1.06	98.42	97.97
X-Lam	868	2.62	0.02	0.06	1.17	0.23	3.81	44.00	0.12	0.53	38.57	2.35	2.04	1.33	95.51	94.95
X-Lam	868	2.61	0.03	0.08	2.56	0.28	3.86	43.73	0.06	0.60	37.69	2.47	2.39	1.68	96.36	95.65
X-Lam	868	2.65	0.03	0.06	2.12	0.29	3.48	44.07	0.10	0.65	39.47	2.05	2.55	1.59	97.51	96.84
X-Lam	868	2.57	0.03	0.03	1.65	0.26	3.49	45.32	0.10	0.64	39.47	2.01	2.18	1.31	97.75	97.20
Formulas																
Шихта	T°C	Na	Mg	Al	Si	K	Ca	Ti	Mn	Fe	Sr	Nb	Ba	F	O*	O+F
3Lam:1Ne	812	0.12	0.00	0.01	0.05	0.00	0.06	0.91	0.01	0.01	0.82	0.01	0.00	0.10	2.88	2.98
3Lam:1Ne	812	0.12	0.00	0.01	0.04	0.00	0.06	0.93	0.01	0.00	0.83	0.01	0.00	0.13	2.86	2.99
3Lam:1Ne	827	0.07	0.00	0.00	0.00	0.00	0.05	1.00	0.00	0.00	0.85	0.01	0.00	0.02	2.97	3.00
3Lam:1Ne	827	0.08	0.00	0.00	0.00	0.00	0.06	1.00	0.00	0.01	0.83	0.01	0.00	0.01	2.98	2.99
15Lam:8Ne	812	0.08	0.00	0.00	0.01	0.00	0.06	0.96	0.00	0.01	0.86	0.01	0.00	0.10	2.90	3.00
X-Lam	868	0.15	0.00	0.00	0.03	0.01	0.12	0.96	0.00	0.01	0.65	0.03	0.02	0.12	2.91	3.04
X-Lam	868	0.15	0.00	0.00	0.07	0.01	0.12	0.95	0.00	0.01	0.63	0.03	0.03	0.15	2.92	3.07
X-Lam	868	0.15	0.00	0.00	0.06	0.01	0.11	0.95	0.00	0.02	0.65	0.03	0.03	0.14	2.90	3.05
X-Lam	868	0.14	0.00	0.00	0.05	0.01	0.11	0.97	0.00	0.02	0.65	0.03	0.02	0.12	2.93	3.05

The resent electron-microprobe studies of synthetic analogue of tausonite show significant concentrations of fluorine (see table 1). The crystallochemical formula was calculated from the chemical analysis using a basis of 2 structural cationic positions.

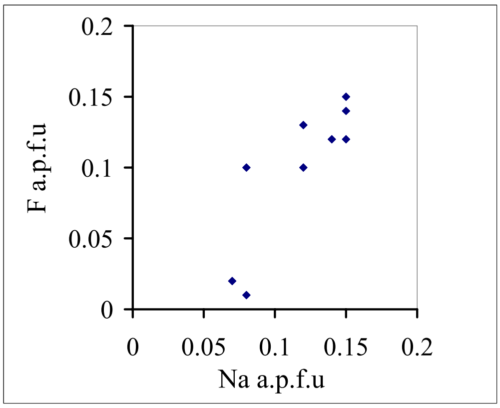

Fig. 1. Correlation between Na and F concentrations in tausonite (by the data of table 1).

Perovskite structure is adopted by many oxides and fluorides. Resently were published also some reports about synthesis of anion-mixing oxide-fluoride solutions with perovskite-structute. For example solid solutions $SrTiO_3$–$NaMgF_3$ and $BaTiO_3$–$NaMgF_3$ containing up to 20% of 20% neiborite ($NaMgF_3$) were crystallized from the NaF-MgF_2 melt [*Talantikite et al., 2004, Talantikite et al., 2010*].

Two polymorph modification of $NaTiO_2F$, were reported in system TiO_2–NaF [*Pavlikov et al., 1975*], but later [*Nalbandyan, 2000*] was shown that roentgenograms of these compositions in Pavlikov's article correspond to mixtures of Na-Ti oxides and NaF. Composition was discredited. Our study show that $NaTiO_2F$ can exist as a component of perovkite-structure solid solution.

Incorporation of fluorine in perovskite structure may result in some geochemical effects:

Perovskite-like minerals may play role in balance of fluorine. For example, F abundance in mantle – 25ppm (McDounald, Sun 1995) is negligible in comparison with F solubility in perovskite. We can suppose that perovskite-type minerals may be the main fluorine phase in lower mantle.

Isomorphic substitution of oxygen by fluorine in perovskite create a negative charge deficit in anion part of structure, it will prevent incorporation of highly-charged cations, like Nb and Ta instead Ti or REE instead Ca and Sr and decrease the distribution coefficients of these elements between perovksite and melt.

Fig 1 show that sodium and fluorine contain equivalent concentrations of Na and F. It allows giving formula $NaTiO_2F$ for sodium end member of solid solution. Fig. 2 show content of sodium minal in tausonite increase with temperature increasment up to 20 mol.%.

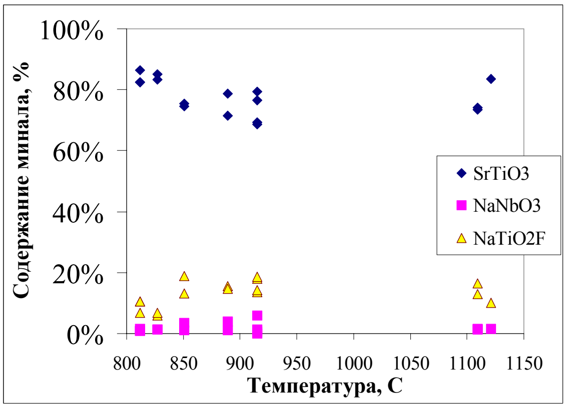

Fig. 2. Dependence of tausonite composition fom temperature ($NaTiO_2F$ calculated by the Na content).

References:

1. Vorobyev, E. I., A. A. Konyev, Y. V. Malyshok, G. F. Afonina, A. N. Sapozhnikov (1984). Tausonite $SrTiO_3$, a new mineral of the perovskite group, *Zap. Vses. Mineral. Obshch.*, 113, 83–9. (in rus.)
2. Zaitsev, V. A., L. D. Krigman, L. N. Kogarko, V. G. Senin (2004). Melting of lamprophyllite group minerals: melting temperature dependence from composition and the element partition between lamprophyllite and melt, *Electronic Scientific Information Journal "Herald of the Department of Earth Sciences RAS"* № 1(22), Informational Bulletin of the Annual Seminar of Experimental Mineralogy, Petrology and Geochemistry, URL:http://www.scgis.ru/russian/cp1251/h_dgggms/1-2004/informbul-1_2004/term-21e.pdf.
3. Zaitsev, V. A., L. D. Krigman, L. N. Kogarko (2004). Experimental study of lamprophyllite-nepheline phase diagram, *Electronic Scientific Information Journal "Herald of the Department of Earth Sciences RAS"* № 1(22), Informational Bulletin of the Annual Seminar of Experimental Mineralogy, Petrology and Geochemistry, URL:http://www.scgis.ru/russian/cp1251/h_dgggms/1-2004/informbul-1_2004/term-20e.pdf.
4. Nalbandyan, V. B. (2000). Interaction of Titanium Dioxide with Sodium Fluoride and Sodium Carbonate, *Russian Journal of Inorganic Chemistry,* vol. 45, No 4.
5. Talantikite, D., Z. Ladjeroud, L. Taïbi-Benziada (2004). Synthesis and Characterization of New Phases with Composition $Sr_{1-x}Na_x(Ti_{1-x}Mg_x)O_{3-3x}F_{3x}$, *Key Engineering Materials*, 264–268, pp.1189–1192.
6. Talantikite-Touati, D., L. Benzïada (2010). Preparation and Characterization of New Oxyfluoride Phases (Ba,Na)(Ti,Mg)(O,F), *Advances in Science and Technology*, 62, 101
7. Pavlikov, V.N., V.A. Yurchenko, E.S. Lugovskaya, L.M. Lpoato, S.G. Tresvyatsky (1975). System NaF-TiO_2, *Journal of analytical chemistry*, vol.20 № 11 pp. 3076–3079 (in rus.)
8. McDonough, W. F., S.-S. Sun, (1995). Composition of the Earth, *Chemical Geology*, 120, 223–253.

Kadik[1] A.A., Litvin[2] Yu.A., Koltashev[3] V.V., Plotnichenko[3] V.G., Tsekhonya[1] T.I., Kononkova[1] N.N. Raman spectra analysis for studing the forms of hydrogen, nitrogen and oxygen dissolution in melting products of the early Earth's mantle

[1] V. I. Vernadsky Institute of Geochemistry and Analytical Chemistry RAS, Moscow
[2] Institute of Experimental Mineralogy RAS, Chernogolovka
[3] Fiber Optics Research Center, RAS, Moscow kadik@geokhi.ru; kvv@fo.gpi.ru

The glasses of composition $(NaAlSi_3O_8)_{80}$–$(FeO)_{20}$ + Si_3N_4 were studed. The analyses and decomposition into the band components of the Raman Spectra of these glasses were made in the region from 2800 to 3800 cm^{-1}. The correlation dependence of these bands on oxygen fugacity, $\Delta \lg fO_2$(IW) permitted us to decompose the bands into some groups and to assign different molecules and complexes in our samples with the help of them.

Key words: experiment, iron- silicate melt, O, H and N dissolution, FTIR and Raman spectroscopy/

Citation: Kadik, A. A., Yu. A. Litvin, V. V. Koltashev, V. G. Plotnichenko, T. I. Tsekhonya, N. N. Kononkova (2012), Raman spectra analysis for studing the forms of hydrogen, nitrogen and oxygen dissolution in melting products of the early Earth's mantle, *Vestn. Otd. nauk Zemle, 4*,

Kadik [1]A. A., Kryukova [1]E. B., Plotnichenko [2]V. G., Kononkova1N. N., Tsekhonya [1]T. I. Spectroscopic analysis of molecular water and hydroxyl groups content in N–O–H ferriferous silicate glasses by FTIR spectroscopy

[1]V. I. Vernadsky Institute of Geochemistry and Analytical Chemistry RAS, Moscow
[2]Fiber Optics Research Center RAS, Moscow *kadik@geokhi.ru;* elena@fo.gpi.ru

The concentration of hydroxyl groups OH^- and molecular water H_2O dissolved in the quenched melt as a function of fO_2 was estimated by the method of Infrared Fourier pectroscopy.

Key words: experiment, silicate melt, dissolution, FTIR spectroscopy, hydroxyl groups, molecular water

Citation: Kadik, A. A., E. B. Kryukova, V. G. Plotnichenko, N. N. Kononkova, T. I. Tsekhonya (2012), Spectroscopic analysis of molecular water and hydroxyl groups content in N–O–H ferriferous silicate glasses by FTIR spectroscopy, *Vestn. Otd. nauk Zemle, 4*,

Studing the forms of dissolution of H, N and O volatiles in glasses – the quenching products of experiments in the system “silicate melt + fused metal Fe phase + Si_3N_4 (1, 3, 5 and 7 wt. %) + H_2» are continued at high pressure and temperature (4 GPa, 1550–1600°C) and low oxygen fugacity (by 2÷4 logarithmic units below the iron–wustite buffer equilibrium $\Delta \lg fO_2$ (IW)).

Table. Parameters for calculating the contents of hydroxyl groups OH^- and molecular water H_2O in L5–L8 albite samples

Run	NBO/*T*	Fugacity $\Delta \log fO_2$(IW)	Density ρ, g/cm³	SiO_2, %***	Al_2O_3, %***	Na_2O, %***	FeO, % ***	H_2O, %***	Impurity							
									OH^-				H_2O			
									α, cm⁻¹	ω, cm⁻¹	ε*	C^{OH}, wt. %	α, cm⁻¹	ω, cm⁻¹	ε**	C^{H2O}, wt. %
L5 d=114 μ	0.384	-2.1	2.4892	63.43	15.87	8.64	9.40	2.66	650	3548	62.4	7.54	186	1632	(49 ± 2) liter/mol·cm	2.74
L6 96μ	0.359	-2.3	2.4725	64.38	15.70	8.78	8.61	2.53	475	3548	62.6	5.53	74	1632		1.10
L7 111μ	0.316	-2.9	2.3516	68.78	15.56	8.13	4.02	3.51	378	3548	63.3	4.58	104	1632		1.63
L8 94μ	0.303	-3.3	2.3143	69.97	15.47	8.45	2.43	3.67	185	3548	63.5	2.27	46	1632		0.73

α, cm⁻¹ – absorption coefficient (IR spectroscopic data) **d,** μ – sample thickness **ω,** cm⁻¹ – frequency
NBO/*T* – structural-chemical parameter describing a degree of melt polymerization
ε, liter/mol·cm – molar absorptivity
ε* – calculation according to [*Mercier et al., 2010*] using our NBO/T data
ε** – according to [*Dixon et al., 1995*]
C^{OH}, wt. % – OH^- content
C^{H2O}, wt. % – H_2O content
$\Delta \log fO_2$(IW) – oxygen fugacity below the iron–wustite buffer equilibrium
*** - ion microprobe data

To estimate the concentration of hydroxyl groups OH^- and molecular water H_2O dissolved in the quenched melt as a function of fO_2 the method of infrared (IR) Fourier-spectroscopy is used. IR transmission spectra were recorded in the frequency region from 350 to 5000 cm⁻¹ with a resolution of 2 cm⁻¹ and a noise level not worse than 0.1 %.

The position and shape of a wide asymmetric absorption band at 3548 cm⁻¹ corresponds to stretching vibrations of hydroxyl groups OH^- and molecules H_2O [*Newman, et al., 1986, Kadik et al., 2004*]. A sharp peak at 1632 cm⁻¹ is a result of deformational (bending) vibrations of molecules H_2O [*Dianov et al., 2005*]. In both peaks a reduction of their intensity is observed with lowering fO_2 within the values of $\Delta \lg fO_2$ (IW) from -2 to -4, so the content of oxidized hydrogen forms OH^- and H_2O decreases in glasses.

The absorption coefficient α of studied glasses has been calculated from thus obtained IR absorption spectra from the 3548 cm⁻¹ and 1632 cm⁻¹ bands corresponding to vibrations of hydroxyl groups OH^- and H_2O molecules. To calculate the extinction coefficient ε thereof we have used its empirical dependence on the structural parameter NBO/*T* obtained in [*Mercier et al., 2010*]. After all the OH^- and H_2O contents in glasses was calculated using the Lambert-Beer law [*Stolper, 1982*]: $C = \alpha \text{ x } 18.02 / \rho \text{ x } \varepsilon$. Thus obtained results are listed in the Table.

Supported by RFFI 11-05-00926, Programs P-28, ONZ-9.

References:

1. Dianov, E. M., V. V. Koltashev, S. N. Klyamkin, A. R. Malosiev, O. I. Medvedkov, V. G. Plotnichenko, A. A. Rybaltovskii, A. O. Rybaltovskii, V. O. Sokolov, S. A.

Vasiliev (2005). Hydrogen diffusion and *ortho-para* conversion in absorption and Raman spectra of germanosilicate optical fibers hydrogen-loaded at 150–170MPa, *Journal of Non-Crystalline Solids,* 351, 49–51, 3677–3684.

2. Dixon, J. E., E. M.Stolper and J. R.Holloway (1995). An experimental study of water and carbon dioxide solubilities in mid-ocean ridge basaltic liquids, Part I: Calibration and solubility models, *Journal of Petrology,* v. 36, N 6, pp. 1607–1631.
3. Kadik, A. A., F. Pineau, Yu. A. Litvin, N. Jendrzejewski, I. Martinez, M. Javoy (2004). Formation of carbon and hydrogen species in magmas at low oxygen fugacity during fluid-absent melting of carbon-bearing mantle, *Journal of Petrology*, 45, 7, 1297–1310.
4. Mercier, M., et al (2010). Spectroscopic analysis (FTIR, Raman) of water in mafic and intermediate glasses and glass inclusions, *Geochimica et Cosmochimica Acta,* v. 74, pp. 5641–5656.
5. Newman, S, E. M. Stolper, S. Epstein (1986). Measurement of water in rhyolitic glasses: Calibration of an infrared spectroscopic technique, *American Mineralogist*, 71, 1527–1541.
6. Stolper, E. (1982). Water in silicate glasses: An infrared spectroscopic study, *Contributions to Mineral Petrology,* v.81, pp. 1–17.

Kadik [1]A. A., Kurovskaya[1] N. A., Ignatjev[1] Yu. A., Kononkova[1] N.N., Krjukova[1] E.B., Dorofeeva[1] V. A., Koltashev[2] V.V. Study of interactions of N–C–H–O volatilies with Fe rich silicate melts at high pressures and fixed hydrogen fugacity

[1]V.I.Vernadsky Institute of Geochemistry and Analytical Chemistry RAS, Moscow kadik@geokhi.ru

[2]Fiber Optics research center RAS, Moscow

Key words: experiment, volatile solubility, silicate melt, oxygen and hydrogen fugacity

It is suggested original construction of the double Pt capsule with the studied specimen in the upper cell and solid oxygen buffer together with H_2O in the lower cell for regulate of the partial hydrogen pressure at the research of volatiles solubility in Fe rich silicate melts at high pressures. With use of the suggested double Pt capsule it is conducted an experiment with ferrobasaltic melt at 1.5 GPa, 1400°C and fH_2, defined by buffer Fe–FeO + 10 mass % H_2O, which allowed to estimate peculiarities of the suggested method of fH_2 regulating in studied silicate systems.

Khodorevskaya L. I. Experimantal study parcial melting of the matabasites in the system H_2O–NaCl

Institute of experimental mineralogy RAS
Khodorevskaya@mail.ru

Experimental studies of interactions amphibolites with pure water (H_2O) and NaCl solutions of different concentrations (X_{NaCl} = 0.1 - 0.5) were conducted at temperature 900°C and at pressures of 5 kbar. A finely ground amphibolite (Amph) is used as a staring material. Major components of the amphibolite are plagioclase, An_{46} (from 25 to 30 mass %), and amphibole, pargasite, (≈ 70 mass %). The amphibole composition is: SiO_2 – 40.80, TiO_2 – 2.17, Al_2O_3 – 11.47, FeO – 17.22, MnO – 0.19, MgO – 9.57, CaO – 11.25, Na_2O – 2.62, K_2O – 1.46, Cl – 0.080, H_2O (loss on ignition) – 1.8; total: – 98.60 mass %. A sample of the initial material (usually from 35 to 40 mg) is lased in the ampoule and poured with the NaCl solution (a sample/solution ratio is 1/10). The ampoules were sealed and withstood at run's P-T conditions during 7 days followed by quenching of rate 100°C/min. The ampoules were gold, keeping transport of iron in/through ampoule walls. Oxygen fugacity f_{O2} was not controlled, we believe that f_{O2} is closed to that of the Ni–NiO buffer [*Helz, 1976*]. When ampoules were opened, compositions of mineral phases, melts and quenched glasses, revealed in amphibolites, were investigated by a local x-ray spectral microanalysis technique using the electron scanning microscope "CamScan MV 2300" supplying with the energy dispersive spectrometer containing the semiconducting Si(Li) detector and the "INCA Energy" software.

Experiments showed that amphibole (Hbl) the major mineral phase, was observed in all runs quite apart from the NaCl concentration in the initial fluid. Rare occurring clinopyroxenes are resulted from interactions of amphibolite and pure water and/or with diluted (from 1 to 5 mass % NaCl) water solutions. Increase of the NaCl concentration in the initial solution expands the field of stability for amphibole. Melt (Gl) resulting from the partial melting of amphibolite forms cement matrix between minerals. The average chemical composition of the melts is following: SiO_2 – 60–62 mass %, Al_2O_3 – 23–25 %, Na_2O – 8–11%, (CaO+MgO+FeO) < 10%. All melts have quartz-norm compositions. As X_{NaCl} in the fluid increases, the melts are enriched in Al_2O_3 and Na_2O and depleted in CaO and K_2O, but their compositions remain the quartz-norm ones. Nepheline-norm melts are only formed at X_{NaCl} > 0.5. Concentration of Cl in the melt increases from 0.4 to 1.5 mass % with increasing X_{NaCl} in the initial fluid from 0.1 to 0.47. The quenched phase (Fl) precipitating from the solution is easily detected and analyzed since it present as spheres with diameters from 20 to 80-150 μm. Chemical compositions of the Gl and Fl melts is practically identical, testifies that at the parameters of 5 кбар and 900°C we are near in area of critical curve glace-fluid.

The initial amphibole in amphibolite is pargasite [*Leake et al.,* 1997]. After experiments, the amphiboles became strong inhomogeneous: they are zoned crystals, in which magnesium concentration increase from the centre of grains to their edges, *i.e.*, Fe^{2+} □ Mg^{2+}. Zoning of amphiboles was observed in the experimental runs with pure H_2O as well as in those with NaCl solution. Amphiboles from runs with high concentrations of NaCl (X_{NaCl} > 0.5) are homogeneous, their compositions is not changed from the centre of grain to its edge. As it follows from the reaction $(Mg,Fe)_{Hbl}$ +H_2O□ $(Mg)_{Hbl}$+Fe(Sol), where Fe(Sol) denotes Fe complexes in the fluid as, increasing activity of water (a_{H2O}) in solution leads to the predominant leakage of Fe from mineral with respect to that of Mg. Another common type of isomorphic substitution in amphiboles is Ca + (Mg, Fe^{2+}) □ Na + (Al, Fe^{3+}). A direct correlation between the NaCl fluid (XNaCl = 0.1–0.5 concentration) and concentration of Cl in the amphiboles (0.1–0.3 mass. %) is observed.

Key words: experiment, amphibolites, *NaCl, fluid*

Reference: Khodorevskaya, L. I. (2012), Experimantal study parcial melting of the matabasites in the system H_2O–NaCl, Vestnik ONZ *RAS, 4*, (doi: .)

Kogarko L.N. Experimental study of high-pressure differentiation of larnite-normative kimberlite melts

Vernadsky Institute of Geochemistry and Analytical Chemistry RAS, Moscow kogarko@geokhi.ru

Experimental study of phase equilibrium of larnite-normative high calcium melilitite demonstrated that merwinite occurs as liquidus phase. With the increasing pressure (up to 20 kb) melilite became unstable and instead of it merwinite ($Ca_3Mg(SiO_4)_2$) started to crystallize as result of reaction $Mg_2SiO_4+Ca_4Si_3O_{10} = Ca_3Mg(SiO_4)_2+CaMgSiO_3$. Therefore high-pressure differentiation of larnite-normative melts will result in fast depletion of residual liquid in Ca and enrichment in silica as compare to low-pressure differentiation when melilite crystallized.

Table merwinite composition

SiO_2	TiO_2	Al_2O_3	FeO	MgO	CaO	total
36.17	0.35	1.15	4.36	10.51	47.45	99.99

Kuzyura[1] A.V., Litvin[1] Yu.A., Vasiliev[2] P.G., Jeffries T.[3], Wall[4] F. Trace elements partitioning at partial melting of diamond-forming peridotite-carbonatite system in experiment at 8.5 GPa

[1]Institute of Experimental Mineralogy RAS, Chernogolovka
shushkanova@iem.ac.ru, fax (496)5249687 tel. (496)5225876
[2] M. V. Lomonosov Moscow State University, Department of Geology, Moscow
[3] Natural History Museum, UK
[4] Cornwall Campus of University of Exeter, UK

The experimental researches at 8.5 GPa and upto 1510°C are directed on studying of geochemical behavior of trace elements in model peridotite-carbonatite system with the composition $[(Ol_{36-60}OPx_{16}CPx_{12-24}Grt_{12-24})_{30}Carb_{70}]_{99}RE_1$. The system was dopped with a mixture of trace elements Li, Rb, Cs, Ba, Th, U, Ta, Nb, La, Ce, Pb, Pr, Sr, Nd, Zr, Hf, Sm, Eu, Gd, Tb, Dy, Y, Ho, Er, Tm, Yb, Lu, Sc, and Zn. Coefficients of interphase participation of trace elements were counted on the base of LA-ICP-MS-analyzes. The main feature of participation picture is that light trace elements (La, Ce, Pr) are distributed mainly into melt phase and olivine, when medium and heavy elements (Nd, Sm, Eu, Gd, Tb, Dy, Ho, Er, Tm, Yb, Lu) go to garnet. Zr, Hf, Y, and Sc are accumulated also in garnet, the rest elements are concentrated in carbonate-silicate melt. An intensive accumulation of light trace elements Li, Rb, Cs, Ba, as well as Th, U, Pb, and Zn is characterized for olivine. It should be noted that clynopiroxene practically doesn't participate in distribution of trace elements. The obtained experimental results testify to participation of trace elements between phases of peridotite-carbonatite system at its partial melting at 8.5 GPa practically doesn't depend on melt composition.

Citation: Kuzyura, A. V., Yu. A. Litvin, P. G. Vasiliev, T. Jeffries, F. Wall v (2012), Trace elements partitioning at partial melting of diamond-forming peridotite-carbonatite system in experiment at 8.5 GPa, *Vestn. Otd. nauk Zemle, 4,*

Kuryaeva R. G., Surkov N. V. Compressibility of the $CsAlSi_3O_8$ glass in the comparison with those for the glasses of albite and orthoclase compositions

Sobolev Institute of Geology and Mineralogy, SB RAS, Novosibirsk
rufina@igm.nsc.ru

The refractive index for $CsAlSi_3O_8$ glass in the pressure range up to 6.0 GPa using a polarization-interference microscope and an apparatus with diamond anvils was measured and the values of compressibility $(d\text{-}d_0)/d$ were estimated. The results were compared with the previous data for the albite ($NaAlSi_3O_8$) and orthoclase ($KAlSi_3O_8$) glasses. Isothermal initial bulk modulus $(K_{t,0})$ of glasses decreases in a series of Na^+, K^+, Cs^+ alkali metal cations. This change in $K_{t,0}$ indicates an increase in the degree of polymerization of the structural network of glasses in the order Na^+, K^+, Cs^+. The increase in $K'_t = \partial K_t/\partial P$ for glasses in the same series can be explained by the fact that the voids are occupied by K^+, Cs^+ cations, which have a larger orbital radius than Na^+, and more strongly inhibit compression. For glass containing Cs^+ a denser packing structure containing three-membered rings of tetrahedra exhibits additional resistance to compression.

Key words: aluminosilicate glasses, high pressures, compressibility of glasses and melts, structure of glasses and melts

Reference: Kuryaeva, R. G., N. V. Surkov (2012), Compressibility of the $CsAlSi_3O_8$ glass in the comparison with those for the glasses of albite and orthoclase compositions, *Vestnik ONZ RAS, 4, (doi:)*

Introduction Silicate and aluminosilicate melts are the dominant phases in the Earth's crust and mantle. Glasses are models of magmatic liquids. Investigation of the properties of various compositions of glasses at high pressures is important for understanding the role of deep melts in magmatic and volcanic processes [*Mysen, 1990; Agee and Walker, 1988*]. A change in the composition of silicate glasses and melts affects the properties that depend on the degree of polymerization, such as viscosity [*Hochella and Brown, 1984; Toplis et al., 1997*] and compressibility [*Webb and Courtial, 1996; Kress, 1988; Kuryaeva and Kirkinskii, 2001*].

For $Al_2O_3 \bullet M(M_2)O \bullet xSiO_2$ glasses with the ratio of $Al_2O_3/M(M_2)O = 1$ the increase in silica content results in an increase in viscosity [*Hochella and Brown, 1984; Toplis et al., 1997*] and compressibility [*Webb and Courtial, 1996; Kress, 1988; Kuryaeva and Kirkinskii, 2001*]. The glasses in which the ratio of $Al_2O_3/M(M_2)O \neq 1$ have a lower compressibility than the glasses with the ratio of $Al_2O_3 /M(M_2)O = 1$, all other things being equal [*Kress, 1988; Kuryaeva 2008*]. Aluminosilicate glasses of the $Al_2O_3 \bullet M(M_2)O \bullet xSiO_2$ composition containing the cations of alkaline earth elements have a lower compressibility compared to those containing cations of alkali metals [Kuryaeva, 2004; Kuryaeva and Surkov, 2010]. And finally, the replacement of the cations Na^+ by K^+ in the $MAlSi_3O_8$ glass was accompanied by an increase in compressibility [*Kuryaeva, 2011*].

In this work we report new results concerning the pressure-dependent behavior of the refractive index and the compressibility for $CsAlSi_3O_8$ glass in the pressure range 0–6.0 GPa . To determine the effect of replacing alkali metal cations in series M = Na, K, Cs on the properties of the $M_2O \bullet Al_2O_3 \bullet 6SiO_2$ glasses, the obtained data were compared with the data for the previously studied $NaAlSi_3O_8$ [*Kuryaeva and Surkov, 2010*] and $KAlSi_3O_8$ [*Kuryaeva, 2011*] glasses.

Experimental technique and results $CsAlSi_3O_8$ glass was synthesized by melting the corresponding oxides and carbonates of special-purity grade at a temperature of 1600–1650 °C for 1 hour in a platinum crucible. Then, the glass was ground in a mortar made from a hard alloy, melted once more, and quenched in water. No annealing of the glass was carried out.

In the experiments polished glass plates 40–50 µm in length and width and 15–20 µm in thickness were used. The samples were polished with diamond pastes on a cardboard.

The refractive index at high hydrostatic pressures was measured by the technique described in detail in our previous works [*Kuryaeva and Kirkinskii, 1994; Kuryaeva and Kirkinskii, 1997*], with the use of the polarizing interference microscope MPI-5 and the apparatus with the diamond anvils. The measuring method of the refractive indices of sample n_x under pressure is based on the pressure-induced change in the optical path difference Φ caused by the sample under study. The optical path difference Φ and the refractive indices of sample n_x and the medium n, in our case a methanol-ethanol 4:1 alcohol mixture, are related by the expression $\Phi=(n_x-n)t$ (1). Expression (1) shows that a decrease in Φ results from the change in the ratio between the refractive indices of sample n_x and the medium n (under pressure, the refractive index of the liquid increases much more rapidly than the refractive index of the glass).

Changes in the relative densities of glass has been calculated from the experimental values of the refractive indices with the use of Mueller photoelasticity theory [*Mueller, 1935*] according to the following equation: $\Delta d/d = 6n\Delta n/(n^2\text{-}1)(n^2+2)(1\text{-}\Lambda)$, where $\Lambda = \text{-} (\Delta R/R_0)/(\Delta d/d)$ is

Mueller strain –polarizability constant. The value of the strain–polarizability constant for aluminosilicate glasses is obtained to be Λ=0.24 [*Kuryaeva, 2004b*]. The Fig.1 demonstrates the values of relative density of the studied glasses within the pressure range up to 6.0 GPa.

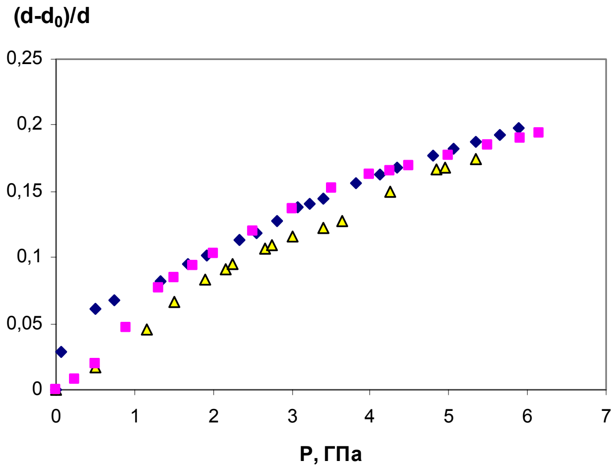

Fig. 1. Pressure dependence of the relative change in the density $(d-d_0)/d$ (compressibility) of glasses: diamonds – $CsAlSi_3O_8$, squares – $KAlSi_3O_8$, triangles – $NaAlSi_3O_8$.

Discussion We analyzed the available literature data on the change in the compressibility of alkali silicate glasses and melts in the series Li, Na, K, Rb, Cs. To compare the compressibilities of various glasses and melts the values of the initial bulk modulus $K_{t(T),0}$ (at normal pressure) and the values of the derivative of the bulk modulus with respect to pressure $K_{t(T)}' = \partial K_{t(T)}/\partial P$ are often used. Using ultrasonic methods in papers [*Rivers and Carmichael, 1987; Webb and Dingwell, 1994*] the values of the initial bulk modulus for alkali silicate [*Rivers and Carmichael, 1987*] and for alkaline titanosilicate melts [*Webb and Dingwell, 1994*] were determined. Obtained in these works data attest to the fact that for melts the initial bulk modulus decreases, therefore, the initial pressure coefficient of the compressibility increases in the order Li, Na, K, Rb, Cs. The change in the bulk modulus is consistent with the decrease in the electronegativity of the cations of alkali metals in the same order. With decreasing electronegativity of alkali metal cations, bonding between Si and O increases in the fragment $\equiv Si–O^-M^+$, but decreases in the adjacent ≡Si–O–Si≡ bonds. Hence, the Si–O network is in general weaker and the rotation around the Si–O–Si bonds is easier [*Revesz, 1972*]. Thus, with the decreasing electronegativity of alkali metal cations in silicate glasses, conformational changes during compression occur with increasing ease.

The same change in the compressibility in the order of Na, K, Cs, are to expected for aluminosilicate systems in which the alkali metal cations compensate the charge in aluminum-oxygen tetrahedra. Aluminosilicate glasses and melts with the ratio of $Al_2O_3/(M)M_2O$=1 contain a number of nonbridging oxygen atoms [*Stebbins and Xu, 1997*] due to the formation of triclusters [*Toplis et al., 1997*]. The smaller the electronegativity of the singly charged cation, the more stable are the aluminum complexes and the lower is the probability of the formation of triclusters and, respectively, the lower is the possibility of forming nonbridging oxygen atoms. That is, for $MAlSi_3O_8$ glasses, the degree of polymerization increases in the series of alkali metals Na, K, Cs, and the compressibility increases in the same order, as well.

Fig. 1 shows that the relative change in the density $(d-d_0)/d$ of the $KAlSi_3O_8$ glass in the pressure range of 2.0–6.0 GPa is indeed greater than that for the $NaAlSi_3O_8$ glass. The values $(d-d_0)/d$ for the $KAlSi_3O_8$ and $NaAlSi_3O_8$ glasses are consistent with the concept of change in the compressibility in a series of alkali metals according to the change in values of electronegativity. A further increase in the compressibility was expected for more polymerised glass of the $CsAlSi_3O_8$ composition. However, the compressibility of the $CsAlSi_3O_8$ glass does not significantly differs from that of the $KAlSi_3O_8$ glass in the pressure range of 2.0–6.0 GPa. This is probably due to unaccounted factors that have an opposite effect on the compressibility, as compared to the effect of the degree of polymerization. To such factors can be attributed an increase in the ionic radius of the cation of alkali metal, which earlier has already been noted in the work [*Kuryaeva, 2011*] and the structure of $CsAlSi_3O_8$ glass, which contains the small rings of the tetrahedrons [*McMillan et al, 1998*].

For all three glasses the initial isothermal bulk modulus $(K_{t,0})$ and the derivative of the bulk modulus with respect to pressure $K_{t(T)}' = \partial K_{t(T)}/\partial P$ in the pressure range with a normal behavior of the pressure coefficient of the compressibility were calculated using experimental data and the isothermal Birch-Murnaghan equation. The isothermal Birch-Murnaghan equation of state has the form:

$P=(3/2)K_{t,0}\{(d/d_0)^{7/3} – (d/d_0)^{5/3}\}\{1 - \frac{3}{4}(4 – K'_t) [(d/d_0)^{2/3} – 1]\}$, where P is the pressure, d is the density of the glass at a pressure P, d_0 is the density of the glass at atmospheric pressure, $K_{t,0}$ is the initial isothermal (at normal pressure and room temperature) bulk modulus of the glass, K'_t is the derivative of the isothermal bulk modulus with respect to pressure. The results of the calculations of $K_{t,0}$ and K'_t are presented in Table 1.

Table 1. The change of $K_{t,0}$, and K'_t for $MAlSi_3O_8$ glasses in the series M = Na [*Kuryaeva and Surkov, 2010*] , K [*Kuryaeva, 2011*], Cs (data from this article.) The orbital radii of alkali metal cations $r_{орб}^{M+}$ are defined in [*Weber and Cromer, 1965*]. The values of the degree of depolymerization *NBO / T* are defined in [*Kuryaeva, 2004a; Kuryaeva, 2011*].

M	$K_{t,0}$ ГПа	K_t'	$r_{орб}^{M+}$ Å	*NBO/T*
Na	16.5	6.0	0.278	0.083
K	13.0	7.0	0.592	0.045
Cs	12.3	7.5	0.921	

The Table 1 shows that in aluminosilicate glasses ($MAlSi_3O_8$) the initial bulk modulus $K_{t,0}$ decreases in the order Na, K, Cs. This trend seems to be explained by the fact that a decrease in the depolymerization of the structural network *NBO/T* (the ratio between the number of nonbridging oxygen atoms and the number of network formers) in the series Na, K, Cs has a dominant influence on the compressibility of the glass at low pressures.

The positive effect of the increasing degree of polymerization in the series of Na, K, Cs on the compressibility of the glasses may be weakened by the influence of factors that contribute to a decrease in compressibility. These factors include: a significant increase in the orbital radius of cations in the series Na, K, Cs, and changes in the glass structure in favor of the formation of three-membered rings for glasses containing Cs. The greater the radius of the cation the greater is its resistance to compression with increasing pressure. A small increase in the derivative of the bulk modulus with respect to pressure (K'_t) in the series aluminosilicate glasses (Table 1) and the convergence of curves $(d\text{-}d_0) / d$–P at pressures above 4.0 GPa for the $NaAlSi_3O_8$ and $KAlSi_3O_8$ glasses (Figs. 1) can be attributed to this factor.

A structure containing three-membered rings (as in the $CsAlSi_3O_8$ glass) is less compressible than the structure containing six-membered rings of tetrahedra (as in the $MAlSi_3O_8$ glasses, M = Na, K) as the three-membered ring have smaller angles of T–O–T bonds and larger packing density compared to six-membered rings [*Revesz, 1972*]. An additional negative influence of the latter factor on the ability of $CsAlSi_3O_8$ glass to shrink under pressure can significantly reduce the increase in the compressibility due to the changes in the degree of polymerization of the structural network. The coincidence of the curves $(d\text{-}d_0)/d$ – P for the $KAlSi_3O_8$ and $CsAlSi_3O_8$ glasses in the pressure range of 2.0–6.0 GPa (Figs. 1) can be explained by the fact that for the $CsAlSi_3O_8$ glass the negative effect of factors that reduce compressibility compensates a positive effect on the compressibility of a higher degree of polymerization of its structure.

Conclusion. For $MAlSi_3O_8$ glasses (M=Na, K, Cs) isothermal initial bulk modulus $(K_{t,\ 0})$ decreases in the series of alkali metal cations Na^+, K^+, Cs^+. This change in $K_{t,\ 0}$ indicates that the degree of polymerization of the structural network of alkali aluminosilicate glasses increases, according to the order Na, K, Cs. The increase in the cation radius in the series of alkali metals and particularly the presence of the three-membered rings in the structure of the aluminosilicate glasses containing Cs have an adverse effect on the increase of the compressibility of the $MAlSi_3O_8$ glasses which is due to the increasing degree of polymerization of the structural network, in the order Na, K, Cs.

References:

1. Agee, C. B., D. Walker (1988). Static compression and olivine flotation in ultrabasic silicate liquid, J. Geophys. Res., V. 93, pp. 3437–3449.
2. Hochella, M.F., G.E. Brown (1984). Structure and viscosity of rhyolitic composition melts, *Geochim. Cosmochim. Acta*, V. 48, pp. 2631–2640.
3. Kress, V.C., Q. Williams, I.S.I. Carmichael (1988). Ultrasonic investigation of melts in the system Na_2O—Al_2O_3—SiO_2, *Geochim. Cosmochim. Acta,* V. 52, pp. 283–292.
4. Kuryaeva, R.G. (2004a). Degree of polymerization of aluminosilicate glasses and melts, *Fiz. Khim. Stekla,* V. 30, pp.212–224 [*Glass Phys. Chem.,* (Engl. Transl.) V. 30, pp. 157–166].
5. Kuryaeva, R.G. (2004b). Effect of high pressure on the refractive index and density of natural aluminosilicate glasses of alkali basalt composition in the SiO_2–Al_2O_3–TiO_2–Fe_2O_3–P_2O_5–FeO–MnO–CaO–MgO–Na_2O–K_2O system, *Fiz. Khim. Stekla,* V. 30, pp.713–724 [*Glass Phys. Chem.*, (Engl. Transl.) V. 30, pp. 523–531].
6. Kuryaeva, R.G. (2008). Influence of pressure on the refractive index and relative density of glasses in the CaO–Al_2O_3–SiO_2 system, *Fiz. Khim. Stekla*, V. 34, No.1, pp. 48-53, [*Glass Phys. Chem*., (Engl. Transl.) V. 34, pp. 37–41].
7. Kuryaeva, R.G. (2009). Effect of pressure on the refractive index and relative density of the CaO $\cdot Al_2O_3 \cdot 6SiO_2$ glass, *J. Non-Cryst. Solids*, V. 355, pp.159–163.
8. Kuryaeva, R.G. (2011). Refractive index and compressibility of the $KAlSi_3O_8$ glass at pressures up to 6.0 GPa, *Fiz. Khim. Stekla*, V. 37, pp. 329-339, [*Glass Phys. Chem*., (Engl. Transl.) V. 37**,** pp. 243–251].
9. Kuryaeva, R.G., V.A. Kirkinskii (1994). Measuring a refractive index at high pressure in a diamond anvil cell, *Prib.Tekh. Eksp.,* V.37, No.6, pp. 166-172 [*Instrum. Exp. Tech.,* (Engl. Transl.) V. 37, pp. 774–778].
10. Kuryaeva, R.G., V.A. Kirkinskii (1997). Influence of high pressure on the refractive index and density of tholeiite basalt glass, *Phys. Chem. Minerals,* V. 25, pp. 48–54.
11. Kuryaeva, R.G., V.A. Kirkinskii (2001). Influence of the degree of oxygen-silicon framework bonding on properties of silicate glasses at high pressures, *Geokhimiya,* V.39, No. 3, pp. 349–352, [*Geochim. Int.*, (Engl. Transl.) V. 39, No. 3. pp. 307–310].
12. Kuryaeva, R.G., N.V. Surkov (2010). Behavior of the refractive index and compressibility of albite glass at pressures up to 6.0 GPa, *Geokhimiya,* No. 8, pp. 887–893, [*Geochim. Int.,* (Engl. Transl.) V.48, No. 8. pp. 835–841].
13. Kushiro, I. (1981). Change in viscosity with pressure of melts in the system CaO–Al_2O_3–SiO_2, *Carnegie Institution of Washington Year Book,* 1980–1981, pp. 339–341.
14. McMillan, P.F., A. Grzechnik, H. Chotalla (1998). Structural characterization of SiO_2–$CsAlO_2$ and SiO_2–$RbAlO_2$ glasses, *J. Non-Cryst. Solids*, V. 226, pp. 239–248.
15. Mueller, H. (1935). Theory of photoelastisity in amorphous solids, Physics, V.6, pp. 179–182.
16. Mysen, B.O. (1990), Relationship between silicate melt structure and petrologic processes, Earth-Sci. Rev., V. 27, pp. 281–365.
17. Revesz, A.G. (1972). Pressure-induced conformational changes in vitreous silica, J. Non-Cryst. Sol., V. 7, pp. 77–85.
18. Rivers, M.L., I.S.E. Carmichael (1987). Ultrasonic studies of silicate melts, J. Geophys. Res., V. 92, No. B9, pp. 9247–9270.
19. Stebbins, J.F., Z. Xu (1997). NMR evidence for excess non-bridging oxygen in an aluminosilicate glass, Nature, V. 390, pp. 60–62.
20. Toplis, M.J., D.B. Dingwell, T. Lenci (1997). Peraluminous viscosity maxima in Na2O–Al2O3–SiO2 liquids: The role of triclusters in tectosilicate melts, Geochim. Cosmochim. Acta, V. 61, pp. 2605–2612.
21. Waber, J.T., D.T. Cromer (1965). Orbital radii of atoms and ions, J. Chem. Phys., V. 42, pp. 4116–4123.
22. Webb, S., P. Courtial (1996). Compressibility of melts in the CaO–Al2O3–SiO2 system, Geochim. Cosmochim. Acta, V. 60, pp. 75–86.
23. Webb, S.L., D.B. Dingwell (1994). Compressibility of titanosilicate melts, Contrib. Min. Petrol., V. 118, pp. 157–16